Computer Modeling in Engineering & Sciences

Tech Science Press

https://doi.org/10.32604/cmes.2026.082366

ARTICLE

Optimized Sustainable Hybridization Through Holistic Multi-Platform Simulation: Enhancing Dynamic Response in Solar-Wind-Battery Energy Systems

Riad Mollik Babu[1], Md Shafiul Alam[2,*], Md. Hasibur Rahman[3], Mohammad Ali[2], Md. Alamgir Hossain[4] and Md. Arifuzzaman[5]

[1]Department of Electrical & Electronic Engineering, University of Asia Pacific, Dhaka, Bangladesh
[2]Department of Electrical Engineering, College of Engineering, King Faisal University, Al Ahsa, Saudi Arabia
[3]Department of Electrical and Electronic Engineering, Gopalganj Science and Technology University, Gopalganj, Bangladesh
[4]School of Science, Engineering and Digital Technologies, University of Southern Queensland, Toowoomba, Australia
[5]Department of Civil and Environmental Engineering, College of Engineering, King Faisal University, Al Ahsa, Saudi Arabia

*Corresponding Author: Md Shafiul Alam. Email: shafiul@kfu.edu.sa

Received: 14 March 2026; Accepted: 12 May 2026; Published: 30 June 2026

ABSTRACT: The increasing penetration of solar photovoltaic (PV) systems into power grids poses challenges due to their inherent intermittency and variability, which can compromise grid stability and reliability. Hybridizing solar PV with wind energy and battery energy storage system (BESS) offers a promising solution by leveraging resource complementarity and providing fast frequency response. This study presents a techno-economic and environmental assessment of a hybrid renewable energy system. Wind turbines and a BESS are integrated with the existing 7.5 MW Sirajganj Solar PV Power Plant in Bangladesh. The proposed hybrid configuration is evaluated using real-world operational data and site-specific environmental parameters in a multi-platform simulation framework. MATLAB Simulink and DIgSILENT PowerFactory assess dynamic control and steady state stability, and HOMER Pro and openLCA perform techno-economic optimization and environmental impact analysis. Six system configurations were analyzed to determine the most technically reliable and cost-effective solution. The selected configuration includes 7.5 MW of solar PV, 6.5 MW of wind, and an 8 MWh BESS. The setup achieves a levelized cost of electricity (LCOE) of $0.123/kWh, a net present cost (NPC) of $34.5 million, and a 7.4-year payback period. Dynamic simulations show grid compliant operation under disturbances. Frequency remains within (European Network of Transmission System Operators for Electricity) ENTSO-E limits, rate of change of frequency (RoCoF) is reduced relative to the standalone PV plant, and harmonic distortion is mitigated through filtering. PVsyst validates the energy output obtained from HOMER Pro and provides performance ratio and detailed system loss breakdowns for the PV system. A Monte Carlo-based uncertainty analysis validates the robustness of the results. Life cycle assessment (LCA) shows the hybrid system's total global warming potential (GWP) was about 20 times lower than coal and 11 times lower than gas generation. The hybrid solution offers a sustainable model for enhancing renewable energy infrastructure in Bangladesh and similar resource-constrained regions.

KEYWORDS: Hybrid solar–wind–BESS system; grid stability and frequency regulation; Monte Carlo simulation; lifecycle emissions assessment; renewable energy optimization

1 Introduction

Global renewable energy deployment has expanded rapidly in recent years, with renewables now contributing nearly half of the world's installed generation capacity [1]. Solar technology dominates this growth, accounting for the vast majority of new installations and indicating a global shift toward low-carbon power generation. Although renewable capacity has increased significantly, integrating high shares of solar energy remains challenging due to irradiance fluctuation and intermittency [2]. The resulting variability increases demands on grid flexibility, energy storage capacity, and system-stability control. Therefore, improving the quality and reliability of renewable energy generation is crucial for the development and large-scale implementation of renewable energy technologies [3]. Solar and wind are the most abundant renewable energy sources. A hybrid system of solar and wind improves supply reliability and reduces intermittency [4,5]. Such hybridization improves overall system stability and minimizes energy curtailment by using the complementary generation profiles of both resources [6].

The integration of PV and wind power with energy storage can enhance output stability and optimize the economic performance [7]. Studies on community-level smart grid hybrids show notable reductions in both cost and emissions, up to 29.65% annually compared to conventional systems [8]. Advanced strategies such as the cascading power-sharing control (PSC) scheme have been proposed to coordinate PV–wind generation in microgrids. These strategies reduce energy losses and maintain dispatch reliability despite disturbances caused by maximum power point tracking (MPPT) control [9]. Optimization-based methodologies, including mixed-integer linear programming (MILP) and multi-objective models, have also been introduced for hybrid system sizing and operation, considering load requirements, cost constraints, and network interactions [10,11]. These approaches improve design precision but often depend on static assumptions and idealized conditions, which limit real-time control accuracy. Recent studies have also explored forecasting and optimization strategies for residential off-grid PV–BESS. These studies demonstrate improved energy management and cost efficiency under variable load and generation conditions [12]. However, these approaches are primarily limited to small-scale off-grid applications and do not address grid-level dynamics, stability constraints, or hybrid resource integration at the utility scale.

Several techno-economic studies have validated hybrid system performance using simulation tools such as HOMER Pro, and show significant cost and emission reductions for rural and small-scale applications [13]. Research on system design optimization in various regions, including China, India, and Bangladesh, has demonstrated the strong solar–wind complementarity and cost reduction potential of hybrid systems [14–16]. However, most analyses do not consider grid-level operational effects such as voltage stability, frequency regulation, and harmonic distortion.

Further advancements have been made in location-specific optimization and environmental assessment of hybrid PV–wind–BESS [17,18]. While these studies examine battery technology selection, lifecycle costs, and renewable fraction improvement, they often overlook long-term uncertainties such as climate variability, degradation, and grid disturbances. In addition, recent analyses of energy-storage cost modeling [19] focus on establishing unified methods for paring storage technologies and defining cost-improvement targets. However, these models remain limited by simplified cost assumptions and the exclusion of cycling effects on storage lifetime.

Although significant progress has been made, most existing studies remain limited to economic optimization or standalone simulation and fail to integrate dynamic control validation, real-world grid interaction, and life cycle environmental impact assessment. These gaps highlight the need for comprehensive, site-specific hybrid frameworks that combine techno-economic optimization, dynamic simulation, and environmental sustainability analysis.

Bangladesh provides an ideal context for applying hybrid renewable energy frameworks due to its rising electricity demand, strong solar potential, and persistent grid-reliability challenges. Despite ambitious government targets to generate 20% of electricity from renewables by 2030 and 30% by 2041 [20], progress has been slow. Renewable sources currently contribute only a small share of the national energy mix. Solar power dominates, while hydro and wind remain limited. Consequently, hybrid renewable systems, particularly solar–wind configurations, offer a practical pathway to expand renewable capacity, improve reliability and optimize land utilization. Figs. 1 and 2 present the current status of renewable energy deployment in Bangladesh and highlight the installed capacity by source and the proportional share of each technology.

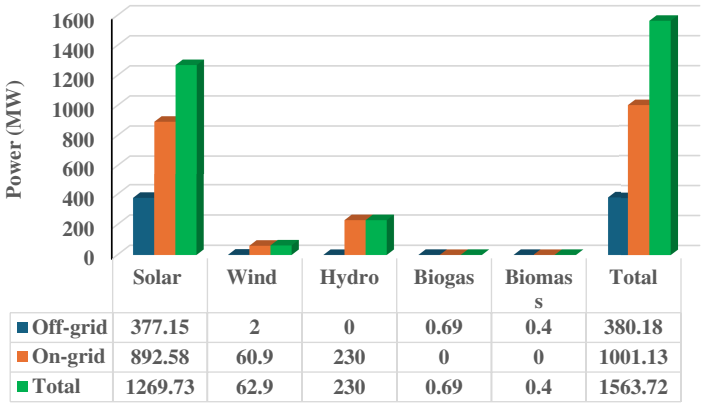

	Solar	Wind	Hydro	Biogas	Biomass	Total
Off-grid	377.15	2	0	0.69	0.4	380.18
On-grid	892.58	60.9	230	0	0	1001.13
Total	1269.73	62.9	230	0.69	0.4	1563.72

Figure 1: Installed renewable energy capacity in Bangladesh by source.

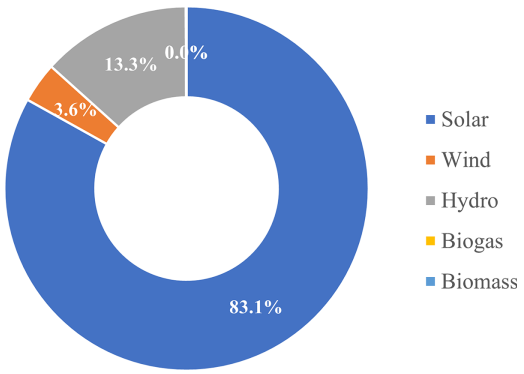

Figure 2: Renewable energy technology share in Bangladesh's installed capacity.

This study evaluates an integrated hybrid renewable energy system that combines solar PV, wind turbines, and BESS with the 7.5 MW Sirajganj Solar PV Power Plant in Bangladesh. The objective is to enhance system reliability, optimize techno-economic performance, and reduce environmental impact under real operating conditions. DIgSILENT PowerFactory, MATLAB Simulink, and HOMER Pro are employed to perform the techno-economic evaluation, while PVsyst is used for validation and to provide additional insights into the PV system.

A review of hybrid renewable energy system studies in Bangladesh over the past decade reveals a consistent pattern. Although techno-economic optimization using HOMER Pro is widely adopted, the literature remains limited in three key aspects. First, most of the reported LCOE for both grid-connected

and off-grid systems typically ranges between $0.239 and $0.392/kWh, which indicates limited cost competitiveness. Second, only a small number of studies incorporate dynamic grid stability analysis, with virtually no integration of harmonic distortion assessment, fault response evaluation, or Rate of Change of Frequency (RoCoF) analysis. Third, comprehensive LCA, particularly the quantification of GWP relative to fossil fuel baselines, remains inadequately addressed. The comparison presented in Table 1 highlights the limitations of existing approaches and underscores the need for an integrated evaluation framework.

Table 1: Comparative benchmarking of hybrid renewable energy system studies in Bangladesh.

Ref.	Location/ Context	System Configuration	LCOE (USD/kWh)	Simulation Tools	Key Limitations/Gaps	Improvement in Present Study
[21]	Bhola	PV-Wind	0.239	HOMER	Economic optimization only; no dynamic grid stability analysis.	↓48.5% LCOE + Grid Compliance Validation
[22]	Nilphamari	PV-Wind-Hydro	0.241	HOMER	Off-grid focus; no frequency response or grid interaction.	↓49.0% LCOE + ENTSO-E Frequency Compliance
[23]	Sitakunda	PV-Wind-Battery	0.363	HOMER	Assumes ideal component performance; no power quality validation.	↓66.1% LCOE + THD Mitigation (<2.14%)
[24]	Chapainawabgonj	PV-Wind-Diesel	0.266	HOMER	Includes diesel backup; no Life Cycle Assessment (LCA).	↓53.8% LCOE + 100% Renewable + LCA
[25]	Tangail	PV-Wind-Hydro	0.281	HOMER	No dynamic response analysis; no resource uncertainty analysis.	↓56.2% LCOE + Monte Carlo Uncertainty Analysis
[26]	Sutabria	PV-Li-Ion Battery-Hydrogen Storage	0.34	HOMER	Stand-alone off-grid system; No wind integration; No dynamic grid stability analysis; No LCA.	↓64.4% LCOE + Grid-Connected Operation + MATLAB/DIgSILENT Validation + Wind Integration + LCA
[27]	Dhaka-Mawa Expressway	Bifacial PV-VAWT-Grid	0.038	HOMER Pro, PVsyst	Utility-scale expressway integration; no dynamic grid stability validation or BESS optimization.	Grid Frequency/RoCoF Analysis + Fault Ride-Through
[28]	Multiple Rural Locations (5 sites)	PV-WT-ZnBr Flow Battery	0.0688	HOMER Pro	Off-grid only; no grid interconnection or dynamic stability assessment.	Grid-Connected Operation + MATLAB/DIgSILENT Validation

(Continued)

Table 1 (continued)

Ref.	Location/ Context	System Configuration	LCOE (USD/kWh)	Simulation Tools	Key Limitations/Gaps	Improvement in Present Study
[29]	Cox's Bazar (Hydrogen)	PV-Wind-Battery-Grid	0.0321	HOMER Pro (CRITIC-TOPSIS MCDM)	Hydrogen production focus; no dynamic grid simulation or harmonic analysis.	Power Quality (THD) Analysis + Fault Protection
[30]	Kunder Char	On-Grid PV-Wind	0.0436	HOMER Pro	No storage system; no frequency response or RoCoF analysis.	Synthetic Inertia + RoCoF Reduction (22%)
[31]	Multiple locations	PV-Wind-Diesel-Battery	0.204	HOMER Pro, MATLAB/Simulink	Focus on dispatch strategy comparison; no THD analysis or LCA.	↓39.7% LCOE + THD Mitigation (<2.14%) + LCA (20× lower GWP vs. coal)
[32]	Rajbari	PV-Wind-Biogas-Battery	0.0207	HOMER Pro, MATLAB	No Grid stability evaluation; no LCA or harmonic distortion analysis.	LCA (GWP: 20× lower than coal) + THD Compliance
[33]	Suburban Areas	PV-wind-biomass	0.0714	HOMER Pro, DIgSILENT PowerFactory	Specialized EV load context; grid stability assessed but no harmonic filtering; no LCA; no PV performance validation.	PVsyst Performance Validation + THD Compliance (<2.14%) + LCA
[34]	Residential Microgrid	PV-Wind-Electrolyzer-Fuel Cell	0.0396	HOMER Pro, MATLAB	Uses MATLAB for dynamic validation; no harmonic distortion analysis; no Life Cycle Assessment (LCA); no PV performance validation.	THD Compliance (<2.14%) + LCA (20× lower GWP vs. coal) + PVsyst Performance Validation + DIgSILENT Steady-State Analysis
This Work	Sirajganj (Grid-Connected)	PV-Wind-BESS	0.123	HOMER, MATLAB/Simulink, DIgSILENT, PVsyst, openLCA	Baseline for holistic comparison	Multi-Platform Validation + Techno-Economic-Environmental Integration

To address these gaps, this study develops an integrated hybrid solar wind BESS model that combines techno-economic optimization with detailed dynamic grid analysis and lifecycle environmental assessment. By incorporating multi-platform simulation and real-world system data, the framework enables a comprehensive evaluation of system performance across economic, technical, and environmental dimensions. The main contributions of this work are summarized as follows:

- A hybrid solar–wind–BESS system is developed for Sirajganj, Bangladesh, leveraging the seasonal complementarity between dry-season solar irradiance and monsoon wind patterns to ensure stable year-round renewable generation.
- A multi-domain assessment framework integrates techno-economic optimization, dynamic grid stability analysis, and life cycle environmental evaluation within a unified workflow. This provides holistic evaluation of hybrid energy systems.
- A comparative analysis of six system configurations is conducted to identify the optimal balance between cost, environmental impact, and system reliability. The results show significant improvements over conventional standalone PV systems.
- Detailed grid impact analysis confirms that the proposed hybrid system substantially enhances voltage stability, frequency response, and power quality, which increases grid hosting capacity and operational resilience under varying load conditions.

2 Methodology

An integrated methodology is adopted to evaluate the feasibility of hybridizing the existing 7.5 MW Sirajganj Solar PV Power Plant. Fig. 3 presents the framework comprising site selection, hybrid system design, techno-economic evaluation, validation, sensitivity analysis, and environmental impact assessment. Key parameters such as energy generation, LCOE, return on investment (ROI), and CO_2 reduction are calculated to assess system viability.

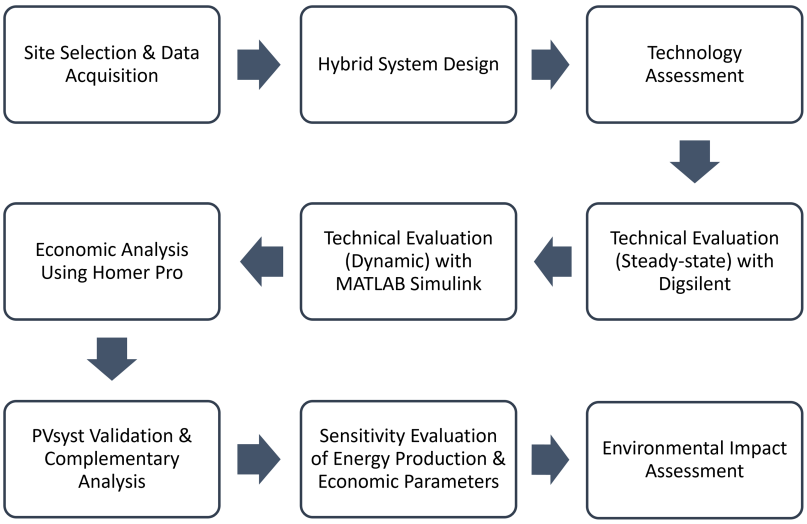

Figure 3: Methodological framework for the design and evaluation of the hybrid system.

2.1 Site Selection

The 7.5 MW grid-connected Sirajganj Solar PV Power Plant is located in Soydabad, Sirajganj District, Bangladesh, at approximate coordinates 24.3905° N and 89.7482° E. It is strategically positioned along the bank of the Jamuna River, one of the largest rivers in the country. The site presents several advantages for renewable energy deployment. Sirajganj was selected for this hybridization study because: first, it hosts one of the largest grid-connected solar PV plants in Bangladesh (7.5 MW), which provides a realistic baseline with actual operational data. Second, while the average inland wind speed is around 3.5 m/s for most parts of Bangladesh, due to its proximity to the Jamuna River, the site yields average wind speeds approximately 40% higher, at about 5 m/s, making wind integration viable [35]. Third, the monthly solar irradiance and wind

speed at Sirajganj show a clear inverse seasonal pattern. Solar peaks during the dry season (March–May) while wind speeds peak during the monsoon (June–August). This makes the site ideal for demonstrating seasonal complementarity (Fig. 4). Although, this is a single-site study, the methodology and findings are transferable to other locations with similar resource complementarity. Fig. 5 shows a satellite view of the Sirajganj Solar PV Power Plant located along the Jamuna River.

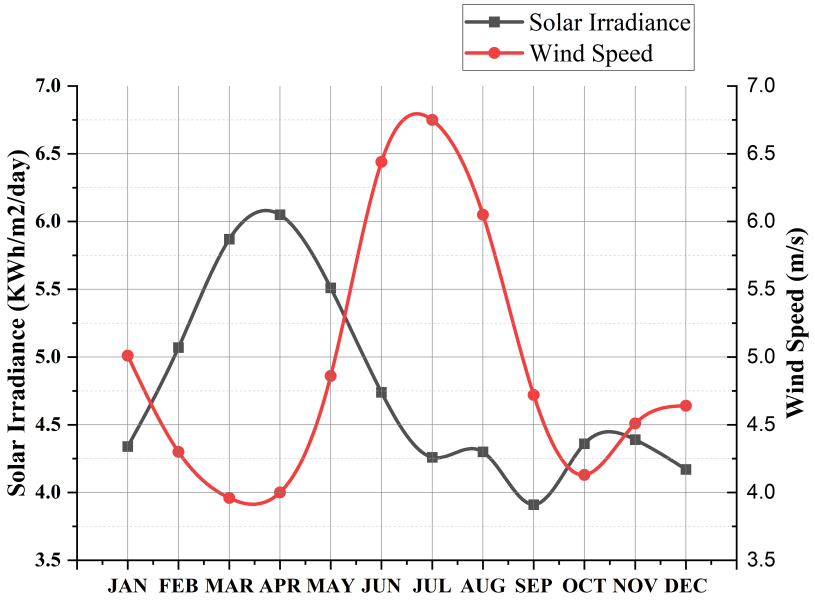

Figure 4: Monthly variation of solar irradiance and wind speed at the Sirajganj project site.

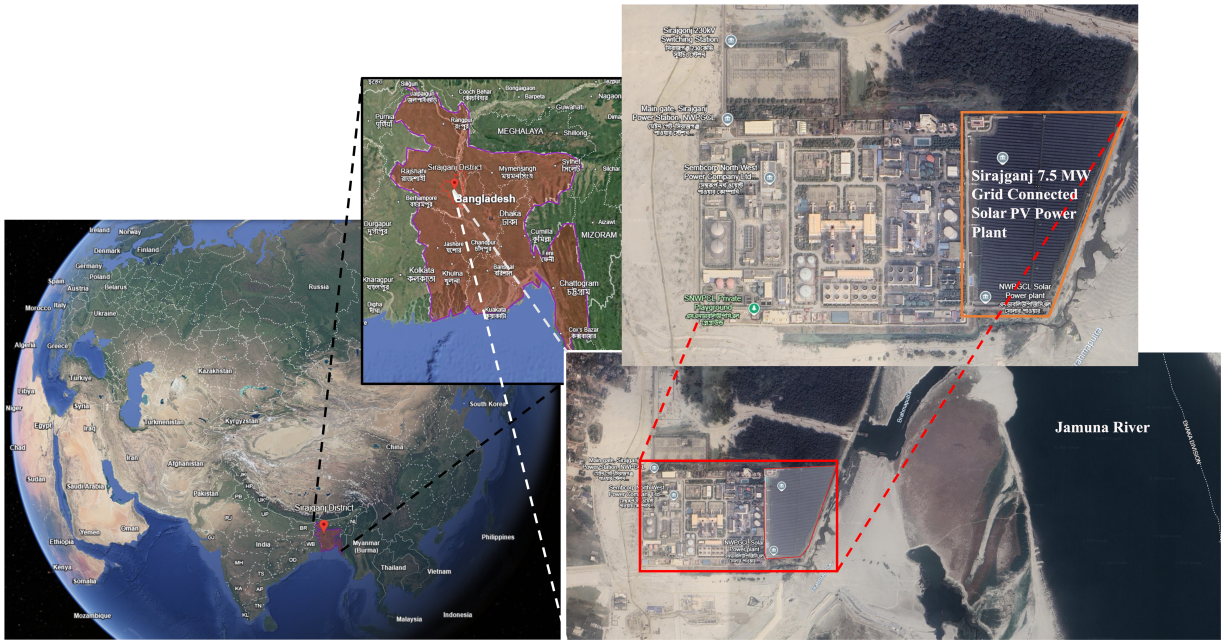

Figure 5: Location of the Sirajganj solar PV plant selected for hybrid system integration.

2.2 Data Collection

This study used both primary and secondary data sources. Key economic parameters for evaluating the Sirajganj Solar PV Power Plant, including total installation cost, sellback price, major system components, funding sources, and loan interest rates, were obtained directly from plant officials. To assess the feasibility of integrating wind energy, technical and operational data were collected from the nearby Sirajganj Wind Turbine Power Project. This practical information supported the design of the hybrid system. Additional economic data for the hybrid configuration, such government subsidies for renewable energy projects, were collected from government agencies including the Sustainable and Renewable Energy Development Authority (SREDA) [36] and the Bangladesh Power Development Board (BPDB) [37]. These institutional datasets are widely used in renewable energy planning studies in Bangladesh due to their regulatory authenticity and national coverage. Other component prices used in the simulations were obtained from similar projects implemented in the country and verified with local equipment suppliers. An annual inflation rate of 6% was adopted based on long-term national trends and recent techno-economic literature for Bangladesh [38]. Similarly, a discount rate of 7.5% was selected in accordance with feasibility studies and international cost of capital benchmarks for emerging economies [39]. Uncertainty in the input parameters was incorporated into the analysis using Monte Carlo simulation to account for their inherent variability and assess its influence on the results. Environmental resource data, including solar irradiance, temperature, and wind speed, were sourced from NASA's Prediction of Worldwide Energy Resources (POWER) [40] database and Meteonorm version 8.1 [41]. These data were validated and cross-referenced using historical records from the Bangladesh Meteorological Department (BMD) [42].

2.3 Resource Assessment

Assessment of local renewable resources is essential for the optimal design of a hybrid solar–wind–BESS system. Fig. 4 presents the monthly variation of Global Horizontal Irradiance (GHI) and wind speed for the Sirajganj region. The solar resource shows strong seasonal variation. GHI peaks at over 6 kWh/m^2/day in April and reaches its lowest level of approximately 3.9 kWh/m^2/day in September, during the monsoon season. These irradiance levels indicate high solar availability during the dry months and lower irradiance during the monsoon season. Wind speed shows an inverse seasonal pattern, increasing significantly during the monsoon months. The site experiences a maximum wind speed of 6.75 m/s in July. The minimum, around 4 m/s, is in March. This seasonal complementarity, strong solar irradiance in summer and higher wind speeds during monsoon, supports continuous renewable energy generation throughout the year.

2.4 System Components

The hybrid solar–wind–BESS system consists of four main components: solar PV modules, inverters, horizontal-axis wind turbines, and a lithium-ion BESS. To ensure consistency with the existing solar PV plant, the same models of solar modules and inverters currently deployed at the Sirajganj Solar Power Plant site were used in this study. The solar array employs monocrystalline LG385N1C-A6 modules manufactured by LG Electronics. This model was selected for its high conversion efficiency of 21.2% and cost-effectiveness, making it suitable for large-scale solar installations. Table 2 presents the detailed specifications of the selected solar module [43]. For power conversion, the Sunny Central 2200 inverter, manufactured by System-Mess- and Anlagentechnik (SMA), is used. This inverter is already deployed in the existing 7.5 MW solar PV plant and is widely adopted across Bangladesh due to its extended service warranty, proven durability, and reliable performance in the regional climate. The technical characteristics of the inverter are provided in Table 3 [44]. For the wind component, the study incorporates the Northern Power Systems (NPS) 100C-28 horizontal-axis wind turbine, rated at 100 kW. This medium-sized turbine was selected based on its compatibility with the

region's wind speeds, as well as its low maintenance requirements and reliable operational profile in hybrid configurations. Unlike conventional geared turbines that require higher cut-in thresholds, the NPS 100C-28 is a Class S turbine specifically optimized for low wind regions [45]. The detailed technical specifications of the selected wind turbine are provided in Table 4. Fig. 6 presents the power curve characteristics of the wind turbine. To complement the renewable generation, 8 units of 1 MWh lithium-ion BESS were integrated, with parameters sourced from the HOMER Pro database. This BESS plays a critical role in load balancing, energy storage, and grid stability. The specifications of the selected battery are summarized in Table 5.

Table 2: Technical and performance specifications of the selected solar PV module.

Specification	Value
Cell Properties	Monocrystalline/N-type
Cell Configuration	60 Cells (6 × 10)
Nominal Max. Power (Pmax)	385 W
Voltage at Maximum Power (Vmpp)	36.1 V
Current at Maximum Power (Impp)	10.67 A
Open Circuit Voltage (Voc)	42.0 V
Short Circuit Current (Isc)	11.43 A
Power Tolerance	+3%
Module Dimensions (L × W × H)	1740 mm × 1042 mm × 40 mm
Module Efficiency	21.2%

Table 3: Specification of the sunny central 2200 inverter.

Input DC	
Max. DC Voltage	1100 V
Min. DC Voltage to Start Feed In	645 V
Max. DC Current	3960 A
MPP(T) Voltage Range	570~950 V
Max. short-circuit current	6400 A
Output AC	
Nominal AC power at cos φ = 1 (at 35°C/at 50°C)	2200 kVA/2000 kVA
Nominal AC power at cos φ = 0.8 (at 35°C/at 50°C)	1760 kW/1600 kW
Nominal AC Voltage Range	308 V/385 V to 462 V
Nominal AC Current	3300 A
Frequency	50, 60 Hz
Max. total harmonic distortion	<3% at nominal power
Min. short-circuit ratio at the AC terminals	>2
Power factor at rated power	1/0.8 overexcited to 0.8 underexcited
Efficiency	98.6%

Table 4: Northern power 100C-28 wind turbine specifications.

Rated Power (kW)	100
Blades length (M)	14
Rotor diameter (M)	28
Rated voltage	400 VAC
Cut-in wind speed (m/s)	2.5
Cut-out wind speed (m/s)	18
Rated wind speed (m/s)	12
Extreme wind speed (m/s)	50.6
Orientation	Upwind, 3 blades
Tower-hub height (M)	37
Design life	20
Drive train	Gearless (permanent magnet direct drive)

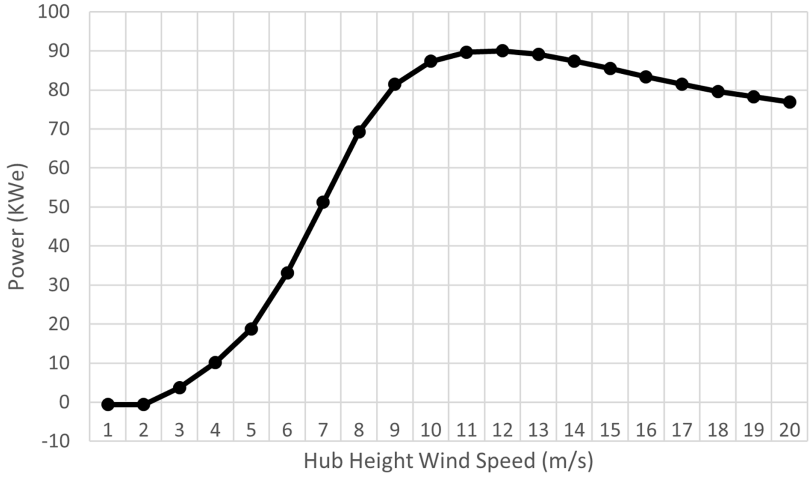

Figure 6: Power curve characteristics of the wind turbine.

Table 5: Technical specifications of the 1 MWh Li-Ion battery.

Parameter	Value
Nominal Voltage	600 V
Nominal Capacity (Energy)	1000 kWh
Nominal Capacity (Charge)	1670 Ah
Roundtrip Efficiency	90%
Maximum Charge Current	1670 A
Maximum Discharge Current	5000 A

2.5 Software for System Simulation

This study employs a multi-software simulation framework to evaluate the technical, economic, and operational performance of the hybrid system. Each software platform is assigned a specific role within an integrated simulation workflow to ensure consistency between economic optimization, dynamic modeling, and grid-level analysis. Input data for all tools are derived from the same validated dataset to maintain consistency across simulations. The steady-state behavior of the system was simulated by DIgSILENT PowerFactory, which provides reliable load flow and grid analysis. The DIgSILENT model incorporates network topology, bus data, line parameters, transformer characteristics, and load profiles to evaluate voltage stability, power losses, and system operating conditions under normal grid operation. However, its environment is less suited for detailed controller-level modeling and dynamic component customization. MATLAB Simulink is used to simulate the dynamic behavior of the hybrid system under varying environmental conditions such as changes in solar irradiance, temperature, and wind speed, and to analyze system performance during fault scenarios. Component-level models of PV arrays, wind turbines, and BESS are developed with control strategies. Time domain simulations are then performed to evaluate system response, controller performance, and transient stability under disturbances. Although MATLAB Simulink is well suited for detailed dynamic and control-oriented simulations, it is less efficient for large-scale steady-state grid analysis. Consequently, MATLAB Simulink alone would not be sufficient to study the full complexity of grid-level interactions. The combined use of both platforms ensures that component-level dynamic behavior and system-wide steady-state performance are evaluated with high accuracy [46–48].

HOMER Pro serves as the primary tool for evaluating economic feasibility and system optimization. It is used to assess multiple system configurations based on resource availability, load conditions, and economic parameters. It supports detailed techno-economic analysis by simulating different hybrid configurations and calculating financial indicators such as the NPC, LCOE, internal rate of return (IRR), and payback period. In addition, PVsyst is employed to assess the performance of the existing solar PV system. This tool validates the energy production and economic results obtained from HOMER Pro by providing a detailed breakdown of performance metrics. The software also offers two key performance parameters that HOMER Pro does not explicitly provide: the performance ratio and a detailed system loss assessment. However, PVsyst is limited to the PV subsystem and it cannot represent interactions among solar, wind, and storage components within the hybrid configuration. To investigate the environmental impact of the proposed system, openLCA software was utilized for lifecycle analysis. Its results depend heavily on the availability and accuracy of lifecycle databases, and certain regional manufacturing or end-of-life pathways may not be fully represented [49–52].

2.6 Technical Performance Analysis

This section presents the operational performance of the hybrid system under both steady-state and dynamic operating conditions. The study conducted the steady state analysis in DIgSILENT PowerFactory to evaluate power flow and overall system stability under normal operating conditions. In contrast, the dynamic analysis was performed in MATLAB Simulink to examine the system's transient behavior under varying solar irradiance, temperature, and wind speed conditions. The BESS operates in a state of charge (SOC) between 20% and 80%. The system discharges during peak demand periods and charges during off-peak hours to support grid stability.

The hybrid configuration was modeled in both simulation platforms. Fig. 7a shows the system architecture and interconnections in the DIgSILENT PowerFactory model, and Fig. 7b presents the MATLAB Simulink model.

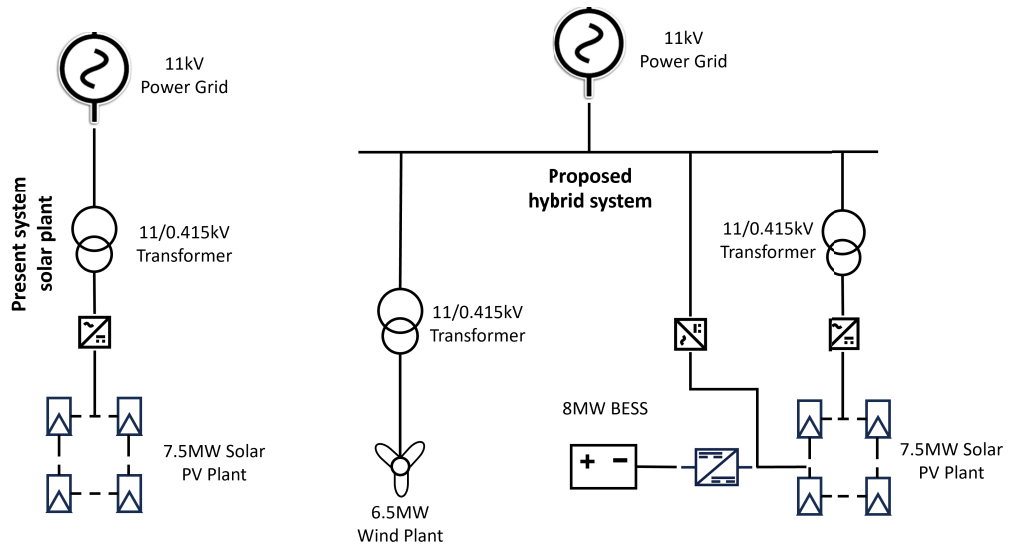

(a)

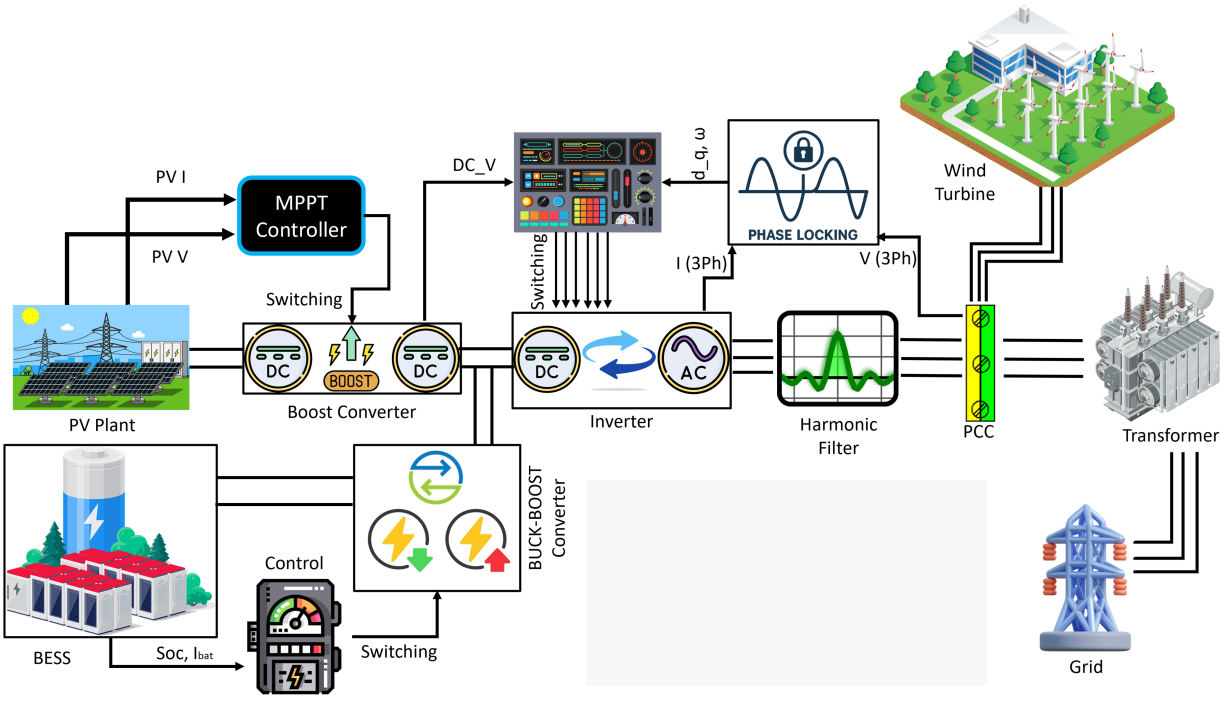

(b)

Figure 7: (**a**) Present vs. proposed system set-up in DIgSILENT PowerFactory. (**b**) Configuration of MATLAB Simulink model of the developed system.

The solar PV plant injects power into the grid by converting its DC output into AC. A synchronizing inverter, modeled in the simulation, performs this conversion. The inverter receives stabilized DC power through a DC–DC boost converter. The converter adjusts voltage and the operating point in response to changes in irradiance and temperature to meet load demand.

A gate driving signal from the MPPT controller regulates the boost converter operation. In this work, a hybrid approach combining the Perturb and Observe (P&O) algorithm and Fuzzy Logic Controller is implemented to enhance tracking performance under dynamic conditions. To overcome the inherent oscillations and slow convergence of standard P&O, a fuzzy logic controller is integrated to adaptively adjust the perturbation step size. The inputs to the fuzzy controller are the change in power (ΔP) and change in voltage (ΔV), while the output determines the optimal perturbation step. An initial step size of $\Delta \approx 0.01$ is used and dynamically tuned to achieve fast convergence with minimal steady-state oscillations. The controller operates with measured inputs of 19.6 A and 606 V, from which instantaneous power is calculated. The resulting duty cycle adjustment of the DC–DC converter ensures accurate MPP tracking and enhances the dynamic stability of the hybrid solar–wind–BESS.

The boost converter operates at a switching frequency of 10 kHz to increase the DC input to 800 V. An inductance of 1.1862×10^{-4} H limits the inductor current ripple (ΔI_I) to 123.89 A. Capacitance of 0.0284 F maintains the output voltage ripple (ΔV_o) within the allowable range. The duty cycle varies within predefined limits. The duty cycle reaches its maximum at the minimum input voltage (≈480 V at low irradiance) and maximum output current (≈9.375 kA at 7.5 MW). The inductance and capacitance values for the boost converter are determined using Eqs. (1) and (2).

$$L = \frac{V_{in} \cdot (1 - D)}{I_{rp} \cdot f_s} \tag{1}$$

$$C = \frac{I_{out} \cdot D}{V_{rp} \cdot f_s} \tag{2}$$

here, L and C are the inductance and capacitance values of the converter. V_{in} and I_{out} indicate the input voltage and output current as well as I_{rp} and V_{rp} represent the ripple voltage and current. After all, f_s denotes the switching frequency, and D is recognized as the converter's duty cycle.

To synchronize the output of the bidirectional inverter with grid power, a Phase Lock Loop (PLL) is developed in the simulation model. To synchronize power, the PLL was designed following the synchronous Reference Frame (SRF) structure. A proportional-integral (PI) controller was used in the system, which generates output with a transfer function shown in Eq. (3).

$$G_{lf}(s) = \frac{V_m K_p s + V_m K_i}{s^2 + V_m K_p s + V_m K_i} \tag{3}$$

where V_m, K_p and K_i are the peak input voltage, proportional gain and integral gain. Therefore, using the damping ratio equal to 0.707, the bandwidth of the PLL is equal to $2.06 * \omega_n$, where $\omega_n = \sqrt{V}_m K_i$ is the natural frequency. Since V_m (p.u.) and k_i were 1 and 212, the PLL bandwidth was 30 Hz and the phase margin was 70 degrees.

To provide the grid angle, the PLL performed a *d-q* transformation on the measured three-phase current and voltage using the "Park transformation". A decoupled current control scheme is implemented in the synchronous reference frame, using Eq. (4).

$$v_{(d,q)} = Ri_{(d,q)} + L\frac{di_{(d,q)}}{dt} - \omega Li_{(d,q)} + v_{g(d,q)} \tag{4}$$

where ω, L, R and $v_{g(d,q)}$ are the grid angular frequency, filter inductance, filter resistance and direct-quadrature component of grid voltage. The inverter voltage references are derived from PI current controllers (shown in Eq. (5)) with cross-coupling compensation terms (ωLi_q and ωLi_d) and grid voltage feed-forward components to enhance dynamic performance.

$$u_d = K_p.i_{(d,q)}(t) + K_i\int i_{(d,q)}(t)\,dt \tag{5}$$

The resulting *d-q* voltage commands are transformed back to abc coordinates and applied to a space vector PWM (SVPWM) modulator. The modulation index is limited within the linear operating range ($m \leq 0.866$), and saturation handling with anti-windup protection is implemented to ensure stable operation under DC-link voltage constraints.

The rotating frame and synchronous phase are utilized in the control unit to generate the pulse width modulation (PWM) signals. The PWM signals control the six metal-oxide-semiconductor field-effect transistor (MOSFET) gates of the inverter as a switching signal.

As the inverter is a nonlinear device, its output contains harmonic distortions. To mitigate these distortions, a harmonic filter composed of inductors and capacitors is included in the simulation. The component values for this filter are calculated using Eqs. (6) and (7).

$$L_f = \frac{0.2 \times V_g}{2\pi 50 \times I_g} \tag{6}$$

$$C_f = \frac{0.05 \times P_i}{2\pi 50 \times V_g^2} \tag{7}$$

The resonance frequency of the Inductor-Capacitor-Inductor (LCL) filter was 2445 Hz to provide attenuation and controllability. Active damping based on capacitor current feedback was implemented to reduce resonance without introducing additional power loss. The grid impedance was varied to represent weak-grid conditions with an Short-Circuit Ratio (SCR) range of 2–10. Stability was evaluated through Bode plot analysis of the closed-loop system. The analysis confirmed a phase margin greater than 45° and a gain margin exceeding 6 dB under critical grid inductance conditions.

To manage energy storage, BESS requires a charge controller. A current control strategy is applied using a DC bidirectional buck–boost converter, which facilitates power transfer in both charging and discharging modes by adjusting voltage levels. The MOSFET gate is derived from a current control signal generated by comparing a threshold voltage with a high-frequency triangular wave. The threshold voltage, which performs the controlling task, is the output of a PI controller that follows the mathematical operation described in Eq. (8).

$$\mathrm{V}_{\mathrm{ctrl}}(t) = k_P.\left(I_{ref} - I_{bat}\right) + k_i\int\left(I_{ref} - I_{bat}\right)d(t) \tag{8}$$

here, V_{ctrl} indicates the threshold voltage, also known as control voltage. k_p, k_i, I_{ref} and I_{bat} are the proportional and integral gains as well as reference and charging/discharging current of the battery. However, the switching signal PWM is generated using Eq. (9).

$$PWM(t) = \begin{cases} 1 & if \mathrm{V}_{\text{ctrl}}(t) > \mathrm{V}_{\text{tri}} \\ 0 & if \mathrm{V}_{\text{ctrl}}(t) \leq \mathrm{V}_{\text{tri}} \end{cases} \tag{9}$$

The proportional (*kp*) and integral (*ki*) gains of the BESS bidirectional PI controller were 0.05 and 10 and the charging and discharging current limits were 4.5 and 6 kA. Fig. 8 shows the nominal discharging current, discharging time at distinct rates with nominal and exponential areas of the discharging curve.

The SOC management strategy maintains SOC between 20% and 80%. The system limits charge and discharge power to 0.5C and applies this limit through converter current saturation. This approach provides smooth power transitions and prevents frequency oscillations near SOC boundaries. A supervisory SOC management algorithm was implemented using a MATLAB Function block to regulate BESS charge and discharge operations. The controller receives SOC and reference power as inputs. Hysteresis thresholds (25% and 75%) prevent control chattering near boundary conditions. Charging and discharging are conditionally activated through persistent logical states. The limited power output is then delivered to the bidirectional converter.

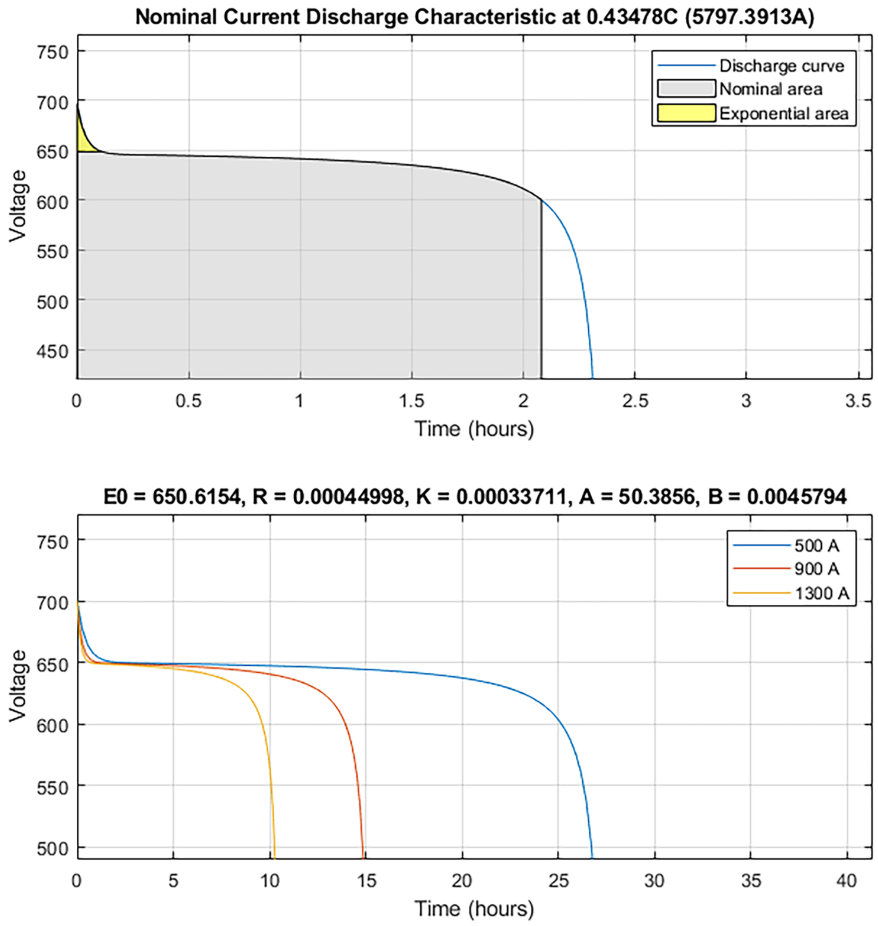

Figure 8: Discharging characteristics of the 8 MWh BESS.

In addition to the solar PV system, a wind turbine system is integrated into the hybrid configuration. The power generated by the turbine depends on wind speed and other parameters, such as pitch angle and tip speed ratio. Fig. 9 illustrates the impact of wind speed on turbine performance. It presents a per unit curve of output power vs. generator rotor speed for different wind velocities.

The frequency stability of the standalone solar PV plant and the hybrid system was assessed. The system was linearized around the operating point to obtain a small-signal transfer function, from which poles and damping ratios were extracted to evaluate dynamic performance. The time-domain frequency response at the point of common coupling (PCC) was simulated under large disturbances, and the rate of change of frequency (RoCoF) was calculated using Eq. (10).

$$RoCoF = \frac{df(t)}{dt} \tag{10}$$

where $f(t)$ is the instantaneous system frequency. This RoCoF, along with the observed frequency deviations, was used to estimate the effective inertia provided by the hybrid system and to compare the damping and transient performance of the standalone and hybrid configurations.

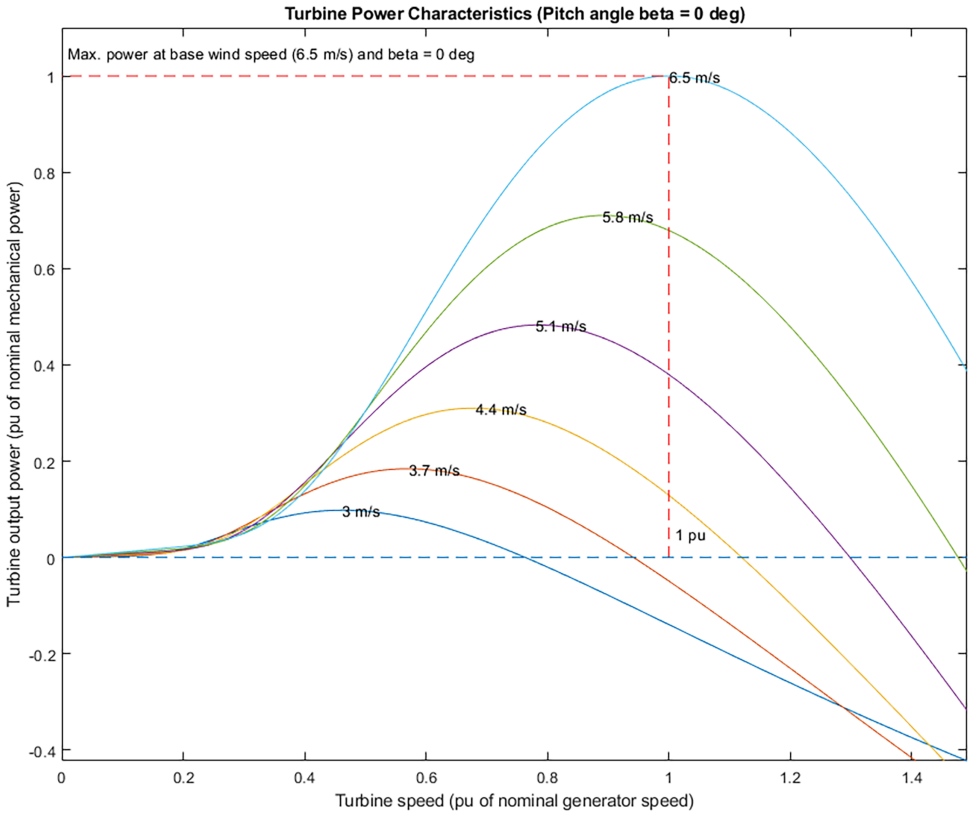

Figure 9: Mechanical power vs. rotor speed curve of the wind turbine under varying wind conditions.

2.7 Economic Analysis

The economic evaluation in this methodology is an important part in assessing the viability of the hybrid system. This evaluation includes the calculation of key financial parameters such as NPC, LCOE, payback period, and ROI.

NPC is used to evaluate the total lifetime cost of the hybrid solar-wind-BESS system. It includes the initial capital investment and the discounted sum of all operation and maintenance costs throughout the system's lifespan. HOMER Pro computes the *NPC* using the expression (11).

$$NPC = C_{cap} + \sum_{t=1}^{T} \frac{C_{om}(t)}{(1+r)^t} \tag{11}$$

where C_{cap} is the capital cost, $C_{om}(t)$ is the annual operation and maintenance cost in the year, r is the discount rate, and T is the project lifetime. This formulation excludes fuel costs, which do not apply to the fully renewable configuration. A lower *NPC* reflects a more economically viable system over the entire lifecycle.

LCOE represents the average cost per kWh of electricity generated by the system over its lifetime. For the grid-connected hybrid solar-wind-BESS system, HOMER Pro calculates *LCOE* using Eq. (12).

$$LCOE = \frac{C_{ann,tot}}{E_{servrd}} \tag{12}$$

where $C_{cann,tot}$ is the total annualized cost and E_{served} is the total annual electricity delivered. This metric allows direct comparison of the cost-effectiveness of different energy configurations.

IRR represents the discount rate at which the NPC becomes zero. It qualifies the expected profitability of the system by equating the present value of all future net cash flows with the total investment cost. HOMER Pro calculates *IRR* using the Eq. (13).

$$0 = \sum_{i=0}^{N} \frac{NC_i}{(1+IRR)^i} \tag{13}$$

where NC_i indicates Net Cast in year i and i is the year index. N is the project lifetime and *IRR* has already been referred. A higher *IRR* indicates a more financially attractive system configuration and greater expected returns over the project's lifetime.

The Payback Period refers to the time required for the proposed hybrid solar-wind-BESS system to recover its initial investment through cumulative annual cash flows or energy cost savings. It is a straightforward economic indicator that helps assess the financial risk and timeline of the system. The payback period is calculated using the Eq. (14).

$$PBP = \frac{TInuC}{CF} \tag{14}$$

where *TInuC* represents the total investment cost of the system and *CF* is the annual cash flow of savings.

2.8 Sensitivity and Probabilistic Analysis

A Monte Carlo simulation with 5000 iterations was performed using the NumPy, Pandas, NumPy Financial, and Matplotlib libraries of Python to evaluate the impact of uncertainties on the energy production and economic performance of the hybrid solar-wind-BESS. Stochastic variations were applied to monthly solar irradiance and wind speed with 5% deviation from the estimated value, as well as economic parameters: electricity tariff (0.17–0.19 $/kWh), O&M cost (1.499–1.561 M$), discount rate (5%–10%), and degradation

rate (0.4%–0.8%/year). For each iteration, annual energy outputs of the solar and wind components were calculated using plant-specific performance ratios and efficiency factors. Sensitivity analysis was conducted by correlating input parameters with energy and economic outcomes. Tornado diagrams are used to identify the most influential factors.

2.9 Environmental Impact Evaluation

The study examines the environmental impact of the hybrid Solar PV-Wind-energy system, with particular emphasis on greenhouse gas (GHG) emission reductions. The analysis evaluates how effectively the hybrid system can displace emissions compared with fossil fuel-based power generation. The GHG reduction rate, expressed in gCO_2/kWh, is calculated using Eq. (15).

$$GHG\_Emission\_Rate = \frac{TGHG\,(gCO_2)}{APG \times LT} \tag{15}$$

where, $TGHG$ = Total greenhouse gas emissions over the system's lifecycle,

APG = Annual power generation,

LT = System lifetime.

2.10 Life Cycle Assessment

OpenLCA [53] performed the LCA of the hybrid system. The analysis aimed to evaluate the environmental burdens of the production, operation, and material flows of the system components. Separate life cycle models were developed for the manufacturing of solar PV modules (7.5 MW), wind turbines (6.5 MW), and BESS (8 MWh). Each model included upstream such as raw material extraction, component manufacturing, assembly, and transportation.

The study utilized multiple impact assessment methods. The ReCiPe 2016 Midpoint (H) [54,55] method was used to estimate GWP, land use, and terrestrial acidification impacts. To assess human toxicity, the Center of Environmental Science-Impact Assessment (CML-IA) baseline method [56,57] was employed due to its detailed treatment of chemical emissions. Ecosystem quality and resource depletion were evaluated using the Eco-indicator 99 framework [58].

All impact categories were analyzed at the midpoint level. The functional unit of the assessment was defined as the total electricity produced by the hybrid system over a 20-year operational lifetime. System boundaries were set from cradle to gate for component manufacturing and cradle to grave for comparative analysis with fossil-based energy generation scenarios. The Greendelta-processed database, European Reference Life Cycle Database ELCD 3.2 [59], was utilized for the processes.

3 Results and Discussion

The performance, feasibility, and sustainability of the hybrid systems were evaluated through an integrated framework combining, techno-economic, and environmental analyses. The hybrid system was modeled to enhance renewable energy penetration at the Sirajganj Solar PV Plant. The BESS provides flexibility to the system.

3.1 Technical Results

The technical performance of the hybrid system was evaluated under both steady-state and dynamic operating conditions. The steady-state analysis, performed in DIgSILENT PowerFactory, examined voltage stability, load flow and power distribution. Additionally, MATLAB Simulink was used to model dynamic behavior, including charging–discharging cycles, frequency response, harmonic mitigation, and fault protection.

3.1.1 Steady-State Performance Analysis

Load flow analysis was performed in DIgSILENT PowerFactory to evaluate the steady-state electrical performance of the system. Table 6 presents the key load flow parameters, including bus voltage profiles, active and reactive power flows, apparent power, and current magnitudes at different nodes of the system, with 33 kV base voltage.

Table 6: System comparison through load flow analysis.

Solar Plant					
Buses	**Voltage (%)**	**MW**	**MVAR**	**MVA**	**Current (kA)**
PV Output	1.05	5.8	1.9	6.1	8.502
Grid Input	1	5.8	1.9	6.1	0.107
Hybrid Plant					
PV Output	1	5.8	1.9	6.1	8.502
Wind Output	1.02	5.5	2.64	6.1	8.961
BESS Output	1	7.03	2.31	7.4	11.102
PCC Bus	1	18.33	6.85	19.6	28.56
Grid Input	1	18.33	6.85	19.6	0.359

For the standalone solar plant, the PV output bus maintains a voltage of 1.05 p.u., delivering 5.8 MW and 1.9 MVAR to the grid with an apparent power of 6.1 MVA. The grid input parameters confirm stable power transfer with minimal line losses, as reflected by the small grid current of 0.107 kA.

The integrated system enhanced power delivery and voltage stability. The wind output bus operates at 1.02 p.u. with an active power of 5.5 MW and reactive support of 2.64 MVAR. The BESS contributes 7.03 MW and 2.31 MVAR at a nominal voltage of 1.0 p.u. The PCC aggregates a total apparent power of 19.6 MVA, with a combined current of 28.56 kA. The grid input remains balanced, shows stable voltage and power levels at all buses. Fig. 10 presents the PV curve analysis for two system configurations: a 7.5 MW solar PV plant and a hybrid system incorporating the same solar capacity along with a 6.5 MW wind turbine and an 8 MWh BESS.

The hybrid configuration shows improved voltage stability. The load bus voltage remains above 0.9 p.u. up to approximately 15 MW of total load, with voltage collapse occurring near 17 MW. In comparison, the solar-only system experiences voltage declines beyond 6 MW, with collapse observed at around 6.4 MW.

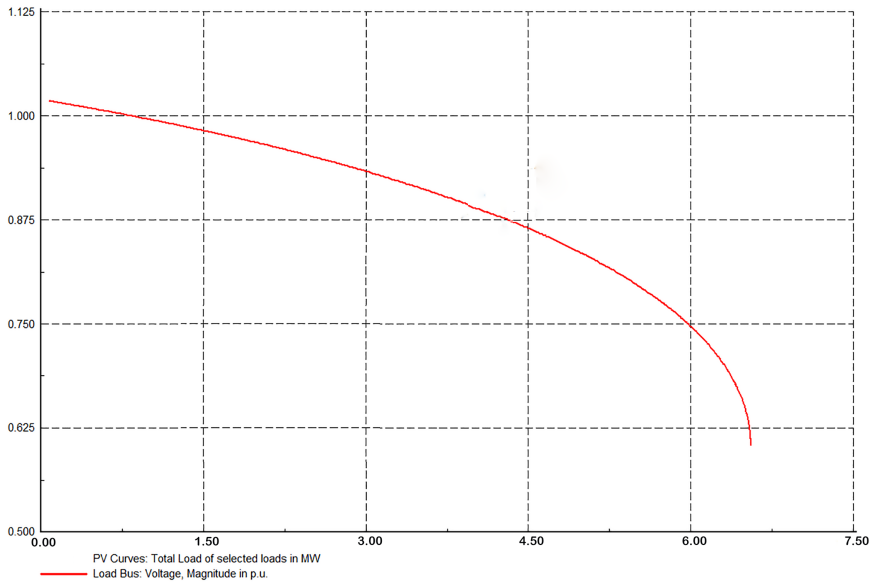

(**a**)

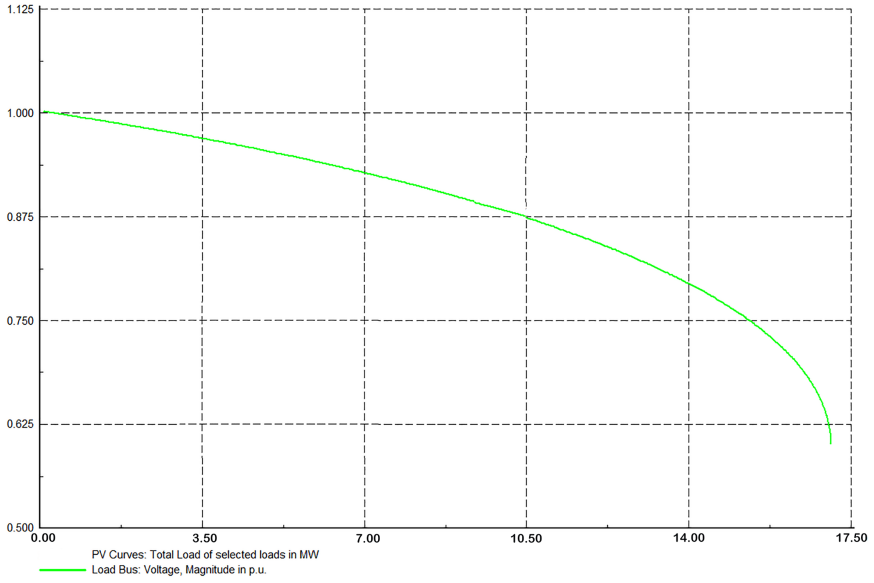

(**b**)

Figure 10: (**a**) Power vs. voltage curve at PCC of the conventional solar PV plant. (**b**) Power vs. voltage curve at PCC of the proposed hybrid plant.

3.1.2 Dynamic Performance Analysis

This section evaluates the dynamic behavior of the hybrid system under varying operating conditions, focusing on power-sharing dynamics, frequency stability, harmonic distortion, and fault response. Time domain simulations assessed system optimization for energy management, grid compliance, and transient stability. The analysis also examined charging-discharging cycles, the impact of harmonic filtering, and the effectiveness of the fault protection scheme.

Charging and Discharging Response of the Hybrid System

The BESS supplies power if consumer demand exceeds the plant's generation capacity during peak hours. This energy is stored during off-peak hours, when the plant generated more power than the demand. As a result, the grid receives a stable and uninterrupted supply of electricity, even during periods of high demand. Positive value of power flow in PCC indicates that the power is injected into the grid. In contrast, the negative flow indicates the absorption of power from the grid. In case of BESS charging and discharging current, the negative flow indicates current flow towards the BESS from the measuring instrument, located at the bidirectional converter input (charging) and the positive flow indicates the opposite event (discharging).

Fig. 11 presents the power generation profiles of the solar PV and wind turbines in response to variations in irradiance and wind speed. The solar PV system delivered 4.65 MW up to 3 s when the incident irradiance was 600 W/m^2. The output dropped sharply to 3 MW as the irradiance decreased to 400 W/m^2 in 0.05 s (from 3 to 3.05 s) at a rate of 4000 W/m^2 per second. The wind turbine provided a relatively constant output of 3.8 MW, with minor initial fluctuations at a wind speed of 5.5 m/s. The BESS contributed 2.7 MW to the system, with a discharging current of approximately 4500 A. The negative direction of power flow indicates that the generated energy was exported to the grid through the PCC. The control system halted discharging when the SOC dropped to 20% at 5.4 s to preserve BESS health. The system showed minor frequency deviations during certain events. The system operated at a nominal frequency of 50 Hz. Three transient spikes were recorded: 49.985 Hz at 0.1 s, 49.989 Hz at 3 s, and 49.992 Hz at 5.4 s. The first spike occurred during grid connection, the sudden drop in irradiance triggered the second, and the third resulted from the disconnection of the BESS due to low charge. According to the European Network of Transmission System Operators for Electricity (ENTSO-E), the normal permissible frequency range is 49.8 to 50.2 Hz, as defined in the ENTSO-E Operation Handbook Policy 1 [60]. The extended short-term deviation range is 47.5 to 51.5 Hz, as documented in ENTSO-E's technical analysis of a major frequency event [61]. These limits are established to prevent load shedding, generator tripping, and cascading failures during transient disturbances. As all observed deviations in this study remain within these permissible thresholds, the system complies with established grid frequency standards.

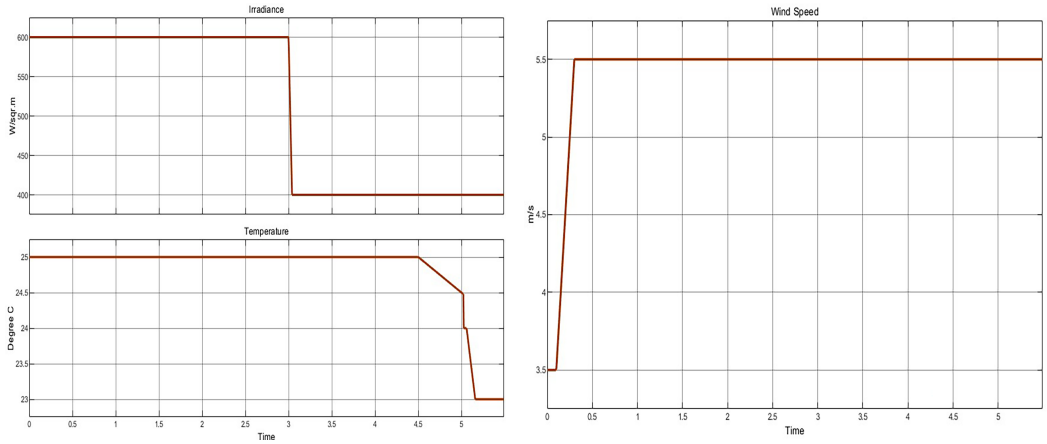

(**a**)

Figure 11: (Continued)

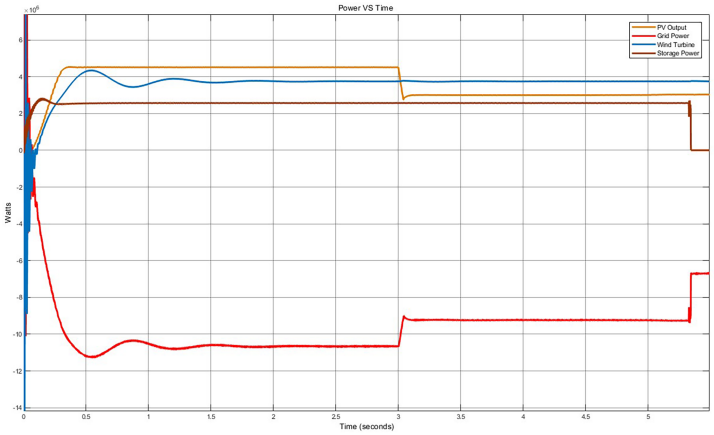

(**b**)

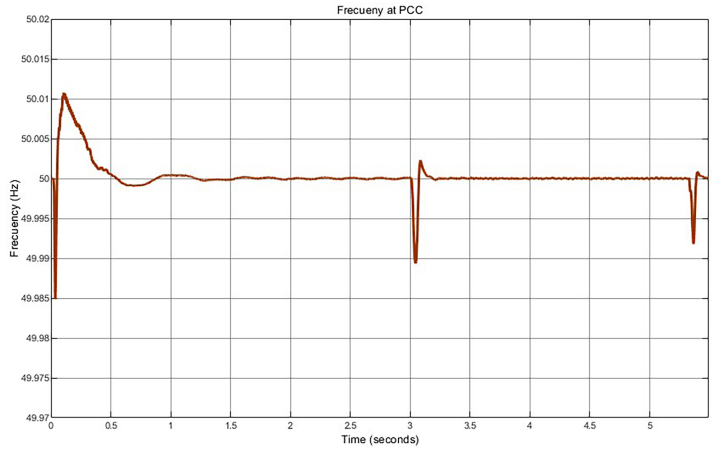

(**c**)

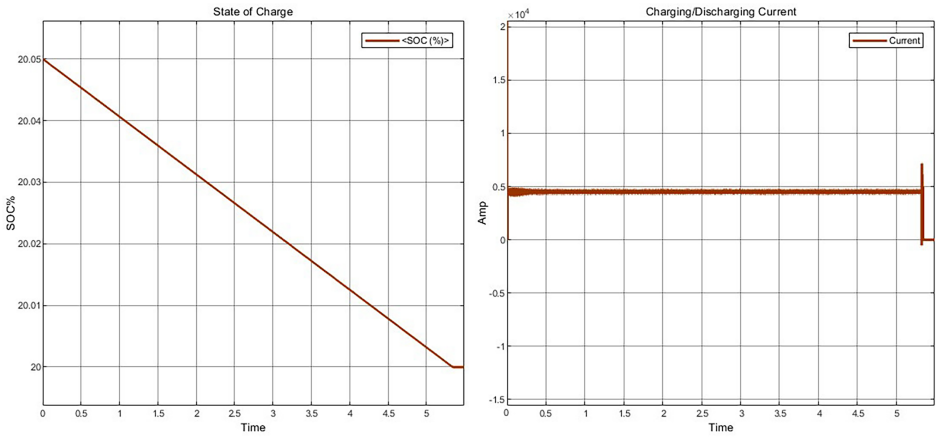

(**d**)

Figure 11: (**a**) Temperature, irradiance and wind speed variation during discharging BESS. (**b**) Power sharing between PV, wind turbine, BESS and grid during discharging. (**c**) Frequency response at PCC in sudden effects. (**d**) State of charge and discharging current of BESS.

Fig. 12 shows the power sharing and system responses of the hybrid plant under charging conditions. In this case, the solar PV system generated 6.2 MW up to 1.3 s when the incident irradiance was 850 W/m^2. The output increased to 7.15 MW as the irradiance rose to 950 W/m^2 in 0.2 s (from 1.3 to 1.5 s) at a rate of

500 W/m^2 per second. The wind turbine delivered a constant output of 3.8 MW at a wind speed of 5.5 m/s. When the wind speed reached 6.5 m/s within 2.5 to 2.65 s at a rate of 6.67 m/s^2, wind generation reached its maximum capacity of approximately 6.5 MW. The BESS began charging at this point, gradually increasing its charging power as the charging current rose from zero to 2800 A. The negative direction of power and current flow from the BESS indicates that it was absorbing power from the grid rather than supplying it. To preserve BESS health, the control system stopped charging when the SOC reached 80% at 4.6 s. Significant frequency deviations were observed during various events. Operating at a nominal frequency of 50 Hz, three transient spikes were recorded: 49.984 Hz at 0.1 s, 50.005 Hz at 2.5 s, and 50.003 Hz at 4.6 s. The first spike occurred during grid connection, a sudden rise in wind speed caused the second, and the third resulted from the disconnection of the BESS after reaching the SOC threshold. Although the irradiance increased by 100 W/m^2 at 1.3 s, no significant frequency deviation was observed, as the increase was gradual. Consequently, the system remains compliant with ENTSO-E frequency standards.

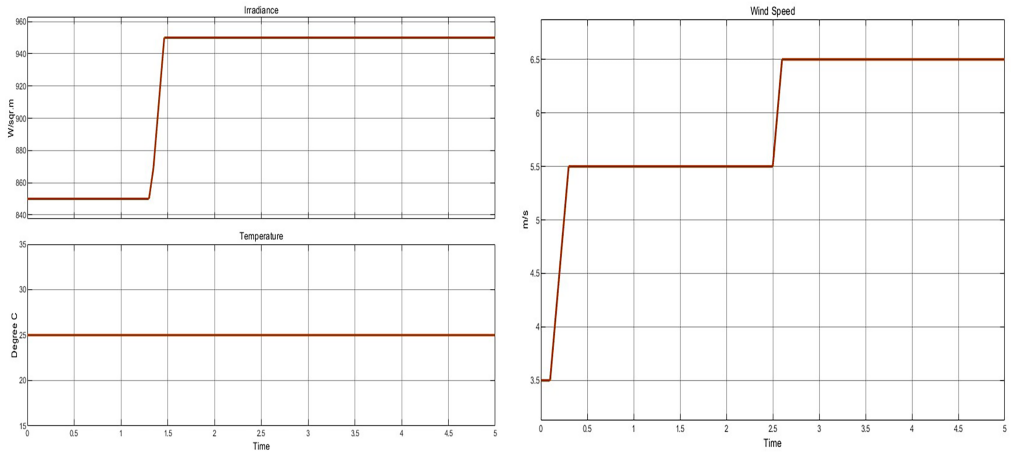

(**a**)

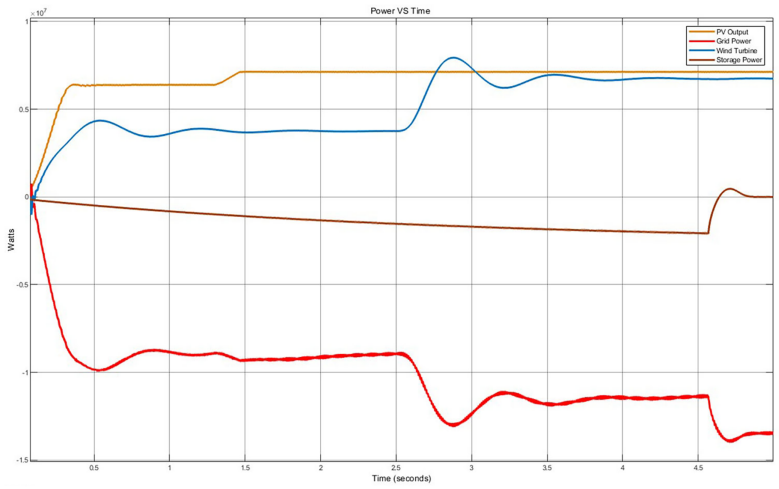

(**b**)

Figure 12: (Continued)

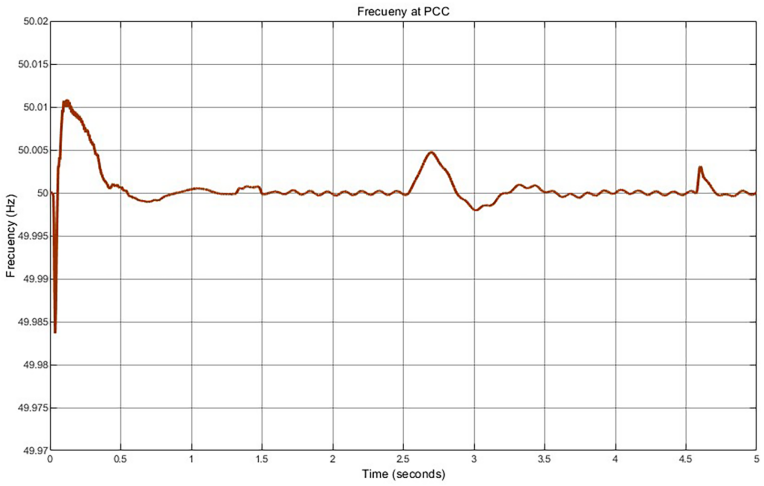

(**c**)

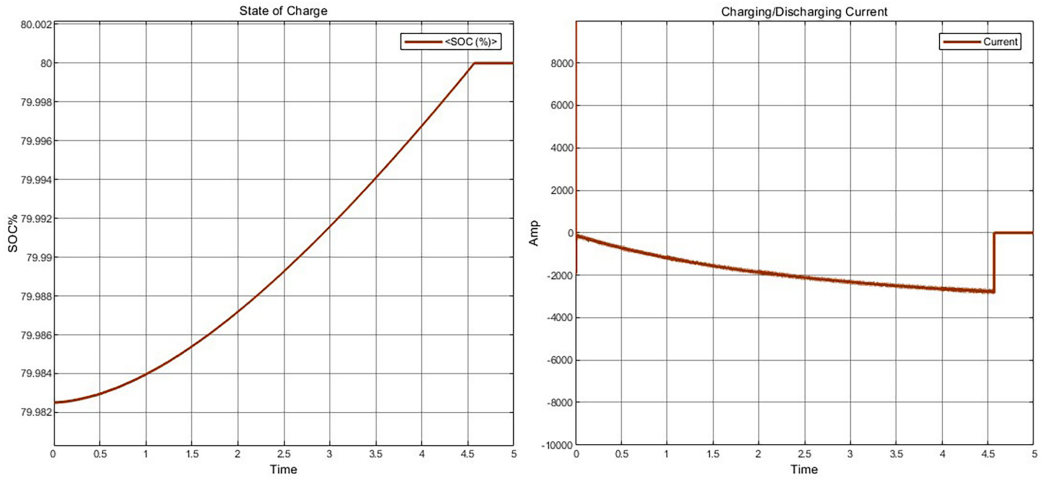

(**d**)

Figure 12: (**a**) Temperature, irradiance and wind speed variation during charging BESS. (**b**) Power sharing between pv, wind turbine, BESS and grid during charging. (**c**) Frequency response at PCC in sudden effects. (**d**) State of charge and charging current of BESS.

Effect of Harmonic Filter in the Simulation Model

The harmonic filter improves the inverter output quality. Fig. 13 illustrates the comparative results. Without the filter, the inverter output shows high distortion with 106.5% THD within 0 to 1000 Hz. In contrast, the use of a harmonic filter effectively mitigates these distortions, with 2.14% THD that aligns with grid standards according to IEEE 519. This demonstrates the filter's critical role in enhancing power quality and system stability in grid-connected hybrid renewable systems.

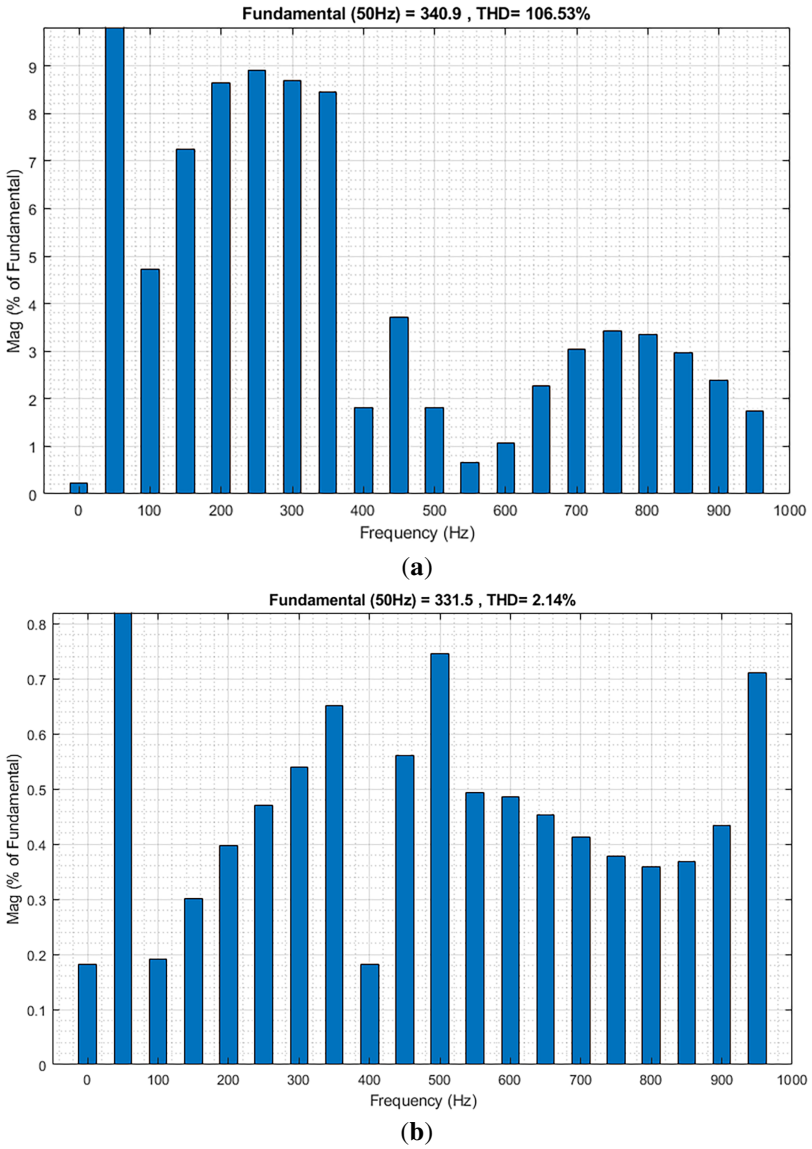

Figure 13: (**a**) Harmonic spectrum of voltage and THD level before using harmonic filter. (**b**) Harmonic spectrum of voltage and THD level after using harmonic filter.

Fault Protection in the Simulation Model

Fig. 14 illustrates the system's fault protection response when subjected to an electrical disturbance. At approximately 1.6 s, a single-phase-to-ground unsymmetrical (L-G) fault occurs in the BESS current path at a point between the BESS inverter and PCC. This causes a momentary surge in storage power flow. Once the fault is detected, the protection mechanism isolates the faulted zone. As a consequence, the BESS current drops to zero, a noticeable distortion appears in the BESS voltage, and a slight deviation is observed in the grid current. The protection system isolates the faulted zone in 0.01 s. This prevents additional instability and maintains operation of the remaining components. The 0.01 s isolation time represents logical trip signal generation and does not include mechanical breaker dynamics. Practical clearing time, including breaker operation, is expected to be 40–60 ms.

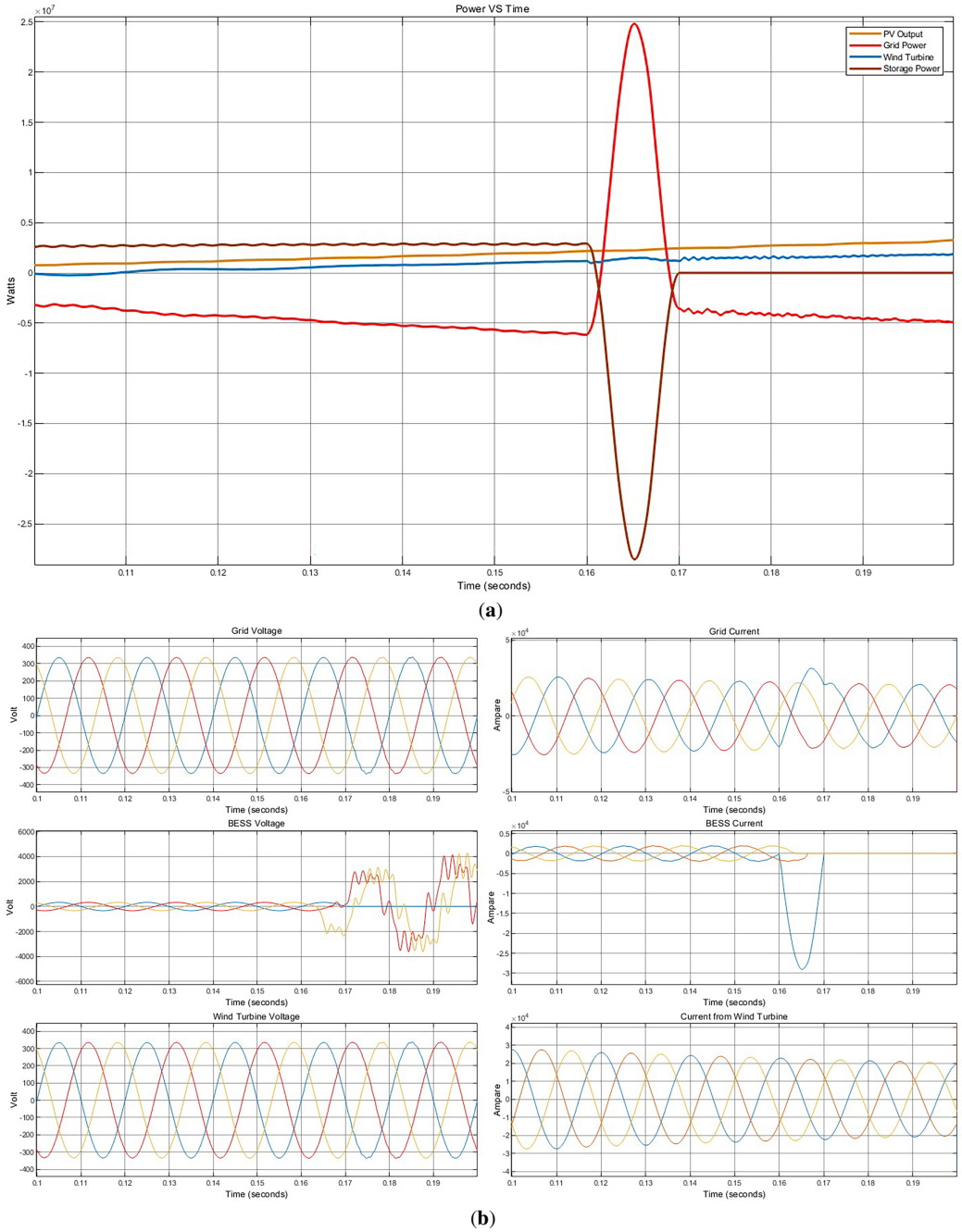

Figure 14: (**a**) Power sharing between the hybrid plant and the grid during fault condition. (**b**) Voltage and current of the grid, wind turbine and BESS during fault condition.

Frequency Stability Analysis

This section compares the frequency response and RoCoF of the solar PV system before and after hybridization with energy storage. This analysis highlights the improvements in inertial response, damping, and transient stability under identical disturbances. In the pre-hybridization scenario (Fig. 15a), the frequency rises to 50.31 Hz at approximately 0.35 s following the disturbance. Although this value remains within the Bangladesh Grid Code normal operating range of 49.5–50.5 Hz (50 ± 0.5 Hz), the corresponding

RoCoF exceeds 9 Hz/s and drops to nearly −4 Hz/s. This reflects weak inertial support and inadequate damping. These large RoCoF excursions indicate inadequate inertial response and damping, resulting in prolonged settling time and sustained oscillations.

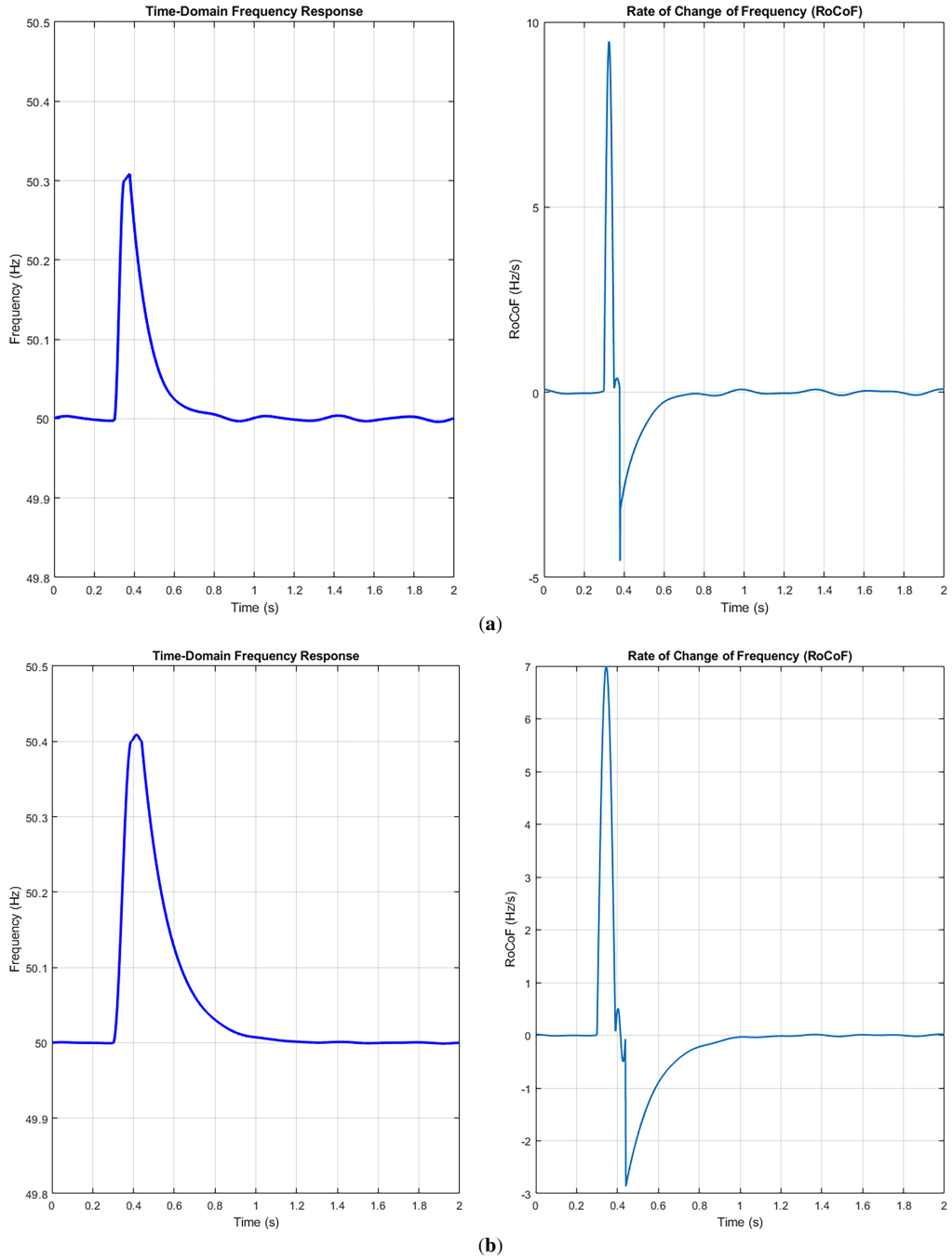

Figure 15: (**a**) Time domain frequency response and RoCoF at PCC of conventional PV system. (**b**) Time domain frequency response and RoCoF at PCC of the hybrid system.

In contrast, the post-hybridization scenario (Fig. 15b) shows improved dynamic performance. Although the peak frequency slightly increases to 50.41 Hz, the maximum RoCoF is reduced to approximately 7 Hz/s

(≈22% reduction). Oscillations decrease and the frequency returns to its nominal value, reflecting enhanced damping and transient stability. The hybrid configuration improves frequency resilience by providing synthetic inertia and fast frequency support.

The dynamic analyses show that the optimized hybrid configuration enhances system performance compared to the standalone solar plant. The coordinated operation of the PV, wind, and BESS ensures balanced power sharing, frequency stability within ENTSO-E limits, and improved transient response. The integration of harmonic filters effectively mitigates waveform distortion, while the protection scheme ensures rapid isolation of faulted sections.

3.2 Economic Result

The economic performance of the hybrid system was evaluated in HOMER Pro. PVsyst validated the HOMER Pro results and provided additional insights into the PV system performance. Key financial indicators, including NPC, LCOE, IRR, and payback period, were assessed to determine the economic feasibility of the system. Six scenarios involving solar PV, wind turbines, BESS, converters, and grid connections were analyzed to identify the optimal configuration. Table 7 presents the six configurations considered for comparison. Fig. 16 shows economic parameters of the major system components in the hybrid configuration, including capital, replacement, and operating costs. Table 8 summarizes the main economic metrics and financial assumptions.

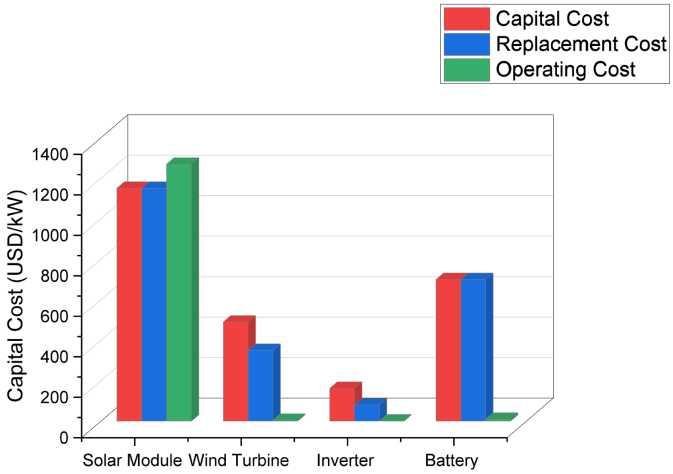

Figure 16: Economic overview of major system components.

Table 7: Summary of different cases.

Components	Case
PV-Wind-BESS-Converter-Grid	A
PV-Wind-Converter-Grid	B
PV-BESS-Converter-Grid	C
PV-Converter-Grid	D
Wind-BESS-Grid	E
Wind-Grid	F

Table 8: Key economic parameters of the hybrid system.

Parameter	Value
Configuration Type	Grid-tied
System Lifetime	25 years
Inflation Rate	6%
Discount Rate	7.5%
Grid Sellback Price	0.1897 $/kWh

3.2.1 Comparative Analysis of System Configurations

Fig. 17 presents a detailed comparative evaluation of six renewable energy system configurations based on NPC, LCOE, initial capital cost, and annual operating cost. These metrics provide the foundation for evaluating the techno-economic feasibility of each system and support the selection of the most balanced configuration.

Case A, integrating solar PV, wind turbines, BESS, converters, and grid connection, is identified as the optimal configuration. It achieves a competitive LCOE of $0.123/kWh along with moderate initial capital investment and an annual operating cost. This configuration represents a balanced solution, combining reliability, renewable diversification, and economic sustainability. In contrast, Case B excludes the BESS and records the highest NPC of $38.1 million, with a slightly lower initial capital cost. Its annual operating cost of $3.97 million reflects the increased dependence on grid transactions and the absence of storage-based load management. Case C, comprising solar PV and BESS, achieves the lowest cost metrics. However, the exclusion of wind turbines limits generation diversity and reduces resilience during periods of low solar irradiance. This limitation reduces the economic benefits of the system. Similarly, Case D includes only solar PV and the grid. Although simpler and cost-effective than hybrid configurations, the lack of storage or secondary generation reduces system independence. Furthermore, Case E combines wind turbines and BESS. Although the site offers moderate wind resource availability, the absence of solar PV reduces generation complementarity and limits the system's ability to deliver consistent power, which negatively impacts both its economic and technical performance. Case F, which integrates only wind turbines and grid connection, has the lowest capital cost of $3.19 million but yields the highest LCOE of $0.162/kWh. This scenario is the least favorable in terms of economic efficiency and renewable utilization. Case A is therefore the most technically resilient and economically balanced configuration. It offers a practical solution for reliable, cost-effective, and sustainable hybrid renewable energy generation.

3.2.2 Optimal Configuration

The techno-economic details of the selected hybrid configuration are presented in Table 9. The system includes a 7.5 MW solar PV system, 6.5 MW of wind turbines, a 6.6 MW inverter, and an 8 MWh BESS. The system generates an annual energy output of approximately 22.10 GWh, including 11.107 GWh from solar PV and 10.995 GWh from wind energy. This hybrid structure ensures a reliable energy supply throughout the year. The configuration achieves a competitive LCOE of 0.123 $/kWh, an NPC of $34.5 million and an annual operating cost of $3.93 million, resulting in profitable grid interaction. An IRR of 30% and an ROI of 26% show favorable investment returns compared with standalone PV or wind installations. Furthermore, a 7.4-year payback period indicates quick capital recovery. Economic results suggest the hybridization effectively recovers higher initial investment through enhanced utilization and reduced intermittency losses.

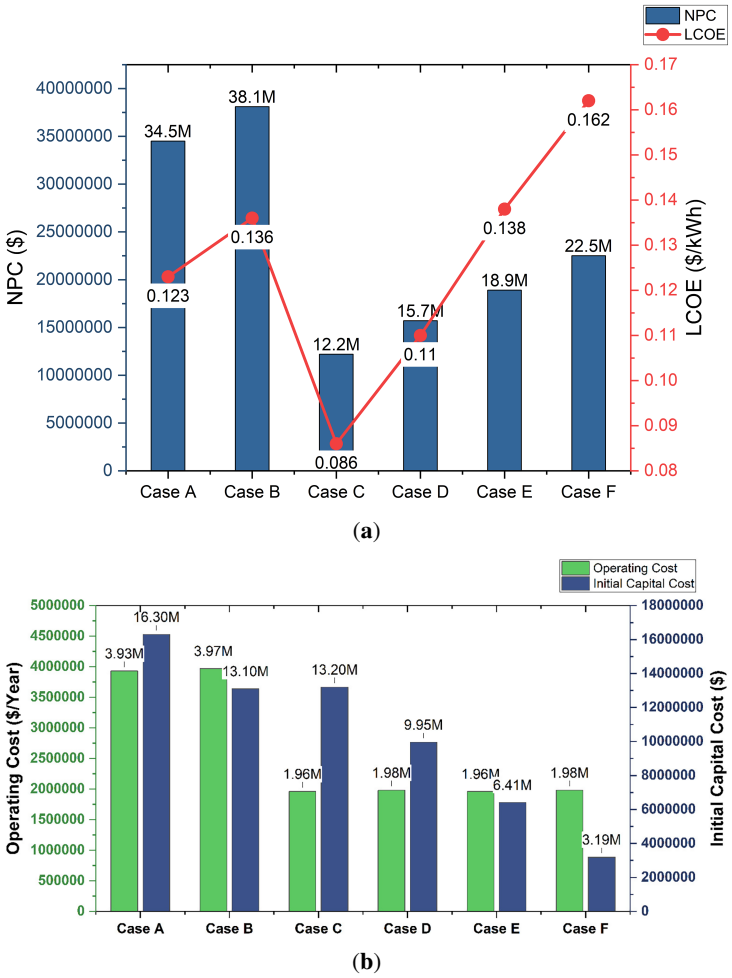

Figure 17: (**a**) Comparative analysis of NPC and LCOE for six hybrid system configurations. (**b**) Comparative financial and operational indicators for different renewable energy systems (RES) configurations.

Table 9: Technical and economic summary of the optimal system configuration.

Category	Parameter	Value
System Architecture	PV (kW)	7500
	Northern Power 100C-28 (kW)	6500
	Inverter (kW)	6600
	BESS	8 MWh
Electrical	NPC ($)	34.5M
	Operating Cost ($/year)	3.93M
Production Summary	PV Production (kWh/year)	11,107,740
	Northern Power 100C-28 Production (kWh/year)	10,995,050
	Total Production (kWh/year)	22,102,790

(Continued)

Table 9 (continued)

Category	Parameter	Value
Economic Metrics	Sellback Price ($)	0.1897
	LCOE	0.123 $/kWh
	IRR	30%
	ROI	26%
	Payback Period	7.4 years

3.2.3 Results of PVsyst Simulation

PVsyst plays an important role in this study due to its specialized focus on the modeling and analysis of solar PV systems. Its advanced analytical capabilities allow detailed evaluation of system efficiency, energy generation, and losses under real-world operating conditions. One of the major advantages of PVsyst is its ability to assess the performance ratio (PR) and calculate detailed system loss. These features are not available in HOMER Pro. PVsyst therefore provides a valuable complement for assessing system performance. In this study, PVsyst validates the PV related simulation results obtained from HOMER Pro. The simulation in PVsyst was conducted using the same input parameters as the HOMER model. This approach ensures consistency and enhances the reliability of the comparative analysis. The summary of PVsyst simulation results is presented in Table 10.

Table 10: Design and performance specification for the Sirajganj solar PV system.

Parameter	Value
Nominal PV Power	7500 kWp
Pnom Ratio	1.14
Number of PV modules	19,482
Modules	1146 string × 17 in series
Unit Nominal Power	2200 kWac
Number of inverters	3
Specific Production	1453 kWh/kWp/year
Produced Energy	10,896 MWh/year
Performance Ratio	76.60%
Module Area	38,632 m^2

3.2.4 Sensitivity and Probabilistic Analysis

Monte Carlo based sensitivity analysis assess the impact of input uncertainties on the hybrid system's economic performance. It shows how variations in resource and financial parameters influence profitability. Table 11 presents the results of the Monte Carlo simulation assessing the impact of parameter uncertainty on energy production and economic performance of the hybrid power plant. The annual energy production demonstrates a mean value of 22,362.23 MWh, with a 95% confidence interval ranging from 21,665.24 to 23,070.71 MWh, which suggests a relatively low variability and reliable generation.

The sensitivity of total energy production to key input parameters is presented in Fig. 18. Mean wind speed shows a strong correlation (0.81) with total output, while mean irradiance has a weaker influence (0.17).

Table 11: Result of sensitivity analysis of energy production and economic parameters.

Result of Monte Carlo Simulation for Energy Production		
Parameter	**Mean Value**	**Confidence Interval (95%)**
Annual Energy Production	22,362.23 MWh	21,665.24 MWh to 23,070.71 MWh
Result of Monte Carlo Simulation for Economic Terms		
Parameter	**Mean Value**	**Confidence Interval (95%)**
NPC	$33,687,729	$24,226,121 to $46,190,695
IRR	31.14%	28.51% to 35.29%
ROI	27.76%	24.37% to 30.83%
LCOE	0.128 $/kWh	$0.1079 to $0.1382
Payback period	7.2 years	7 years to 8 years

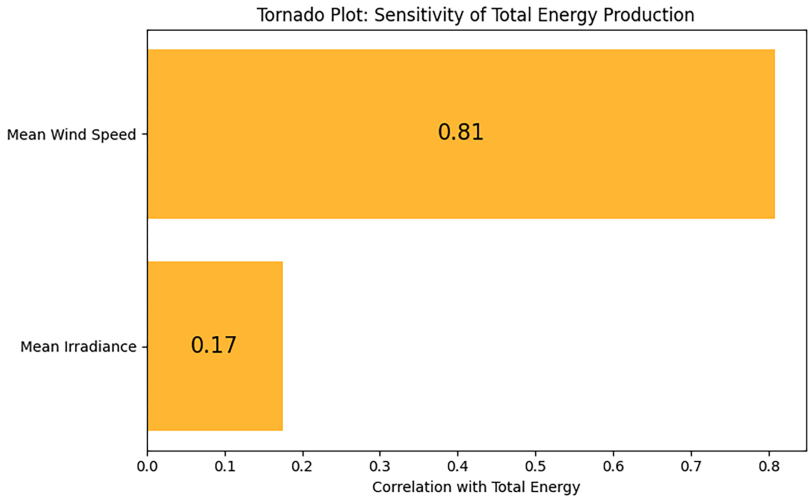

Figure 18: Tornado chart exhibiting sensitivity of energy production of hybrid plant.

Fig. 19 presents the tornado chart illustrating the sensitivity of the NPC to major economic parameters. The discount rate and tariff have the strongest impact on NPC, with the discount rate showing a strong negative correlation and the tariff showing a strong positive correlation. In contrast, the O&M cost and degradation rate have comparatively smaller impacts.

Fig. 20 presents the probabilistic distributions of NPC, IRR, ROI, and LCOE obtained from Monte Carlo simulations. The NPC distribution confirms that most scenarios generate positive returns. Both IRR and ROI show near-normal distributions centered around 30%–32% and 25%–30%, which suggests stable investment outcomes. The LCOE distribution remains narrow, within 0.11–0.13 $/kWh.

The sensitivity and probability analyses show that wind speed and discount rate are the primary factors affecting energy output and economic parameters. The confidence intervals of key metrics such as annual energy production, NPC, and LCOE are narrow.

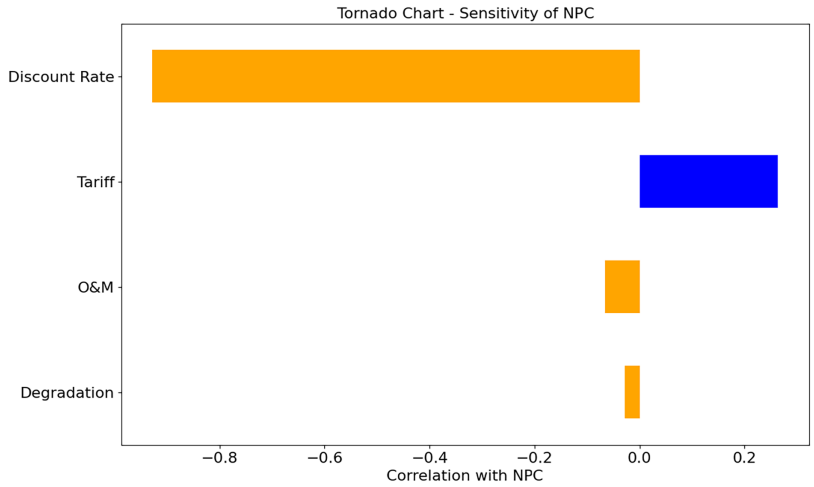

Figure 19: Tornado chart exhibiting sensitivity of NPC for the proposed system.

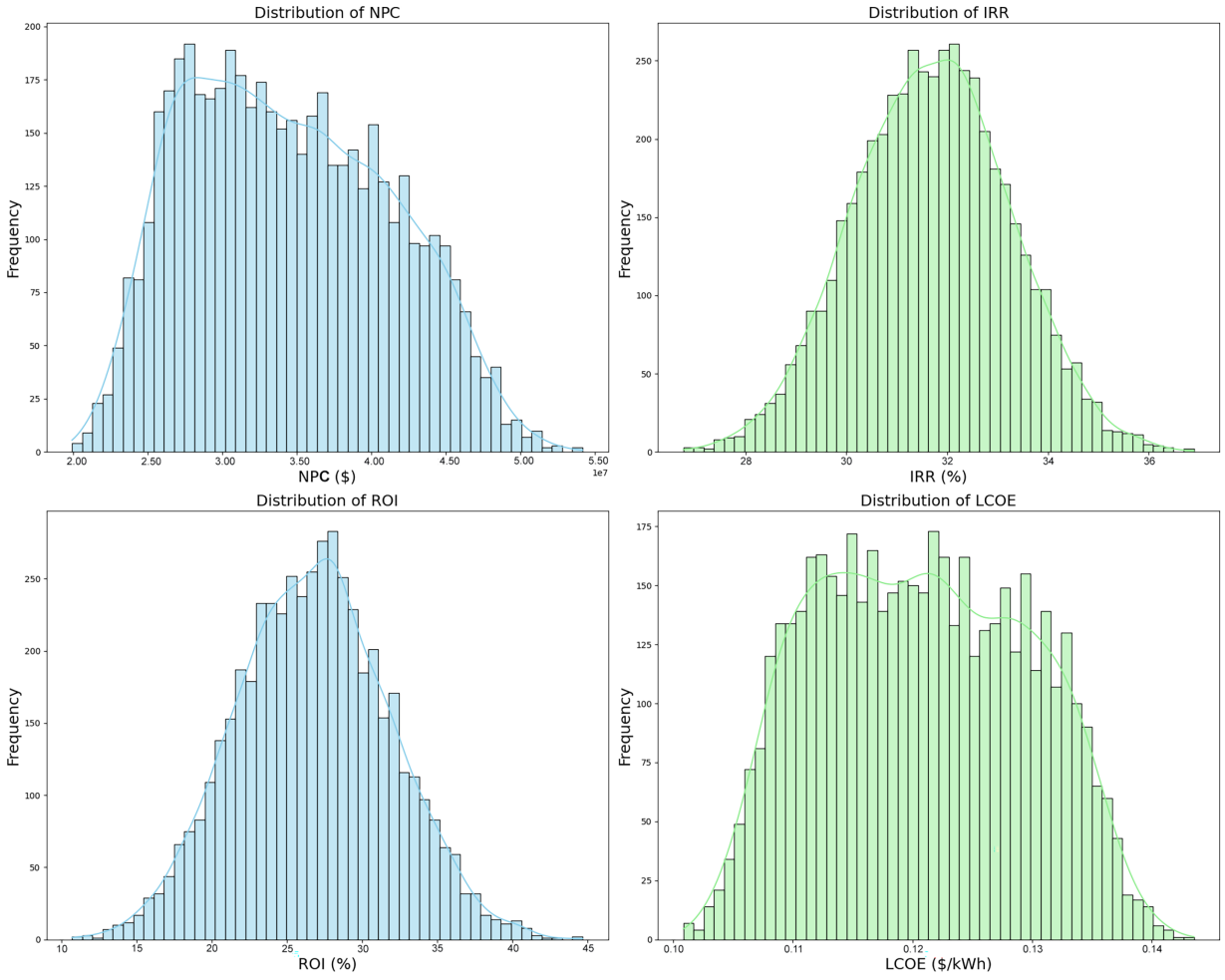

Figure 20: Histogram plot demonstrates probabilistic distributions of economic parameters of hybrid system.

3.2.5 Performance Ratio

The PR is a critical metric for evaluating the efficiency of grid-connected PV systems. It represents the proportion of actual energy delivered to the grid relative to the theoretical energy output under standard test conditions (STC). The performance ratio for a grid-connected PV system is given by:

$$PR = \frac{E\_Grid}{GlobInc \times PnomPV} \tag{16}$$

where E_Grid is the energy injected into the grid, $GlobInc$ the global incident irradiation in the plane of the array, and $PnomPV$ the nominal PV capacity under STC.

Fig. 21 presents the monthly variation of the PR for the solar PV system. The high PR values throughout the year reflect the system's overall efficiency and reliability under diverse operating conditions.

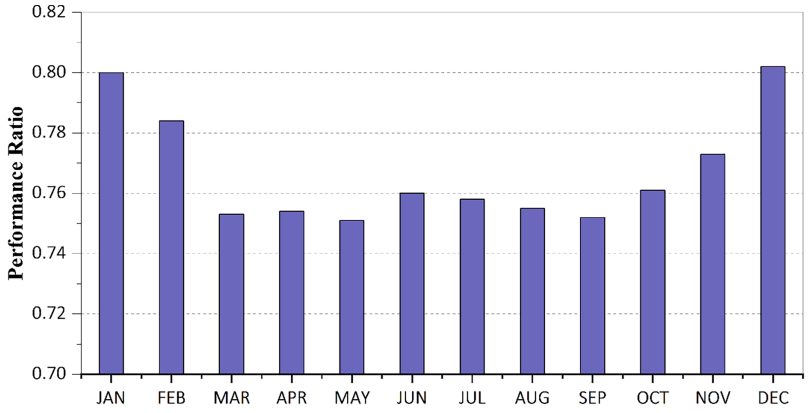

Figure 21: Monthly variation of PR for the grid-connected solar PV system.

3.2.6 Energy Generation Data

Fig. 22 presents the monthly solar energy generation data obtained from PVsyst simulations. It provides a detailed overview of the energy output from the existing PV system throughout the year under real-world environmental conditions.

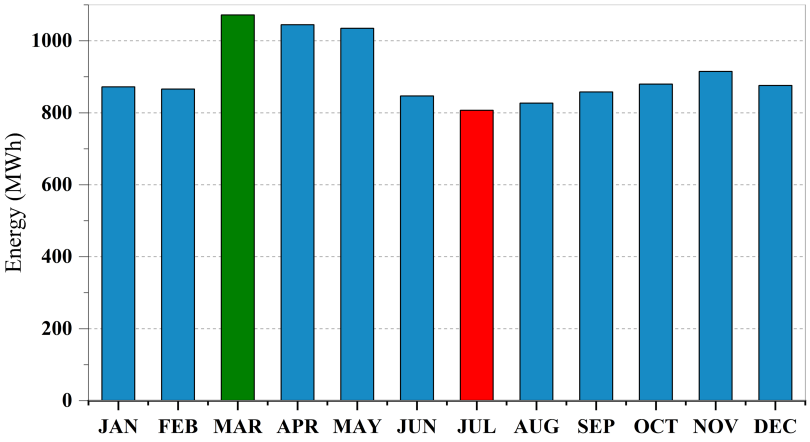

Figure 22: Monthly variation in solar PV energy output.

3.2.7 PV System Loss Assessment

A detailed loss assessment helps identify key areas for performance optimization, particularly in thermal management, module matching, and inverter efficiency improvements. Fig. 23 illustrates the loss distribution of the solar PV system, assessed using PVsyst simulation software. The figure presents a breakdown of the various factors contributing to system energy loss.

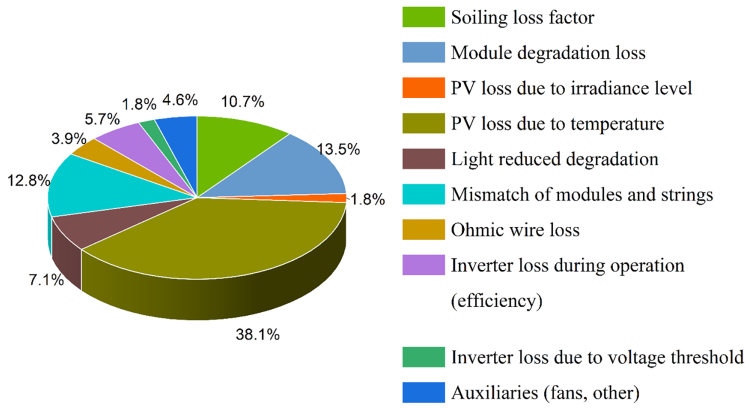

Figure 23: Detailed loss distribution of the solar PV system components.

3.2.8 System Output Analysis

Fig. 24 presents the monthly distribution of system output energy, comparing the total energy generated by the PV array to the amount of energy delivered to the grid. Throughout the year, the energy generated by the PV system exceeds the energy exported, which indicates the presence of system losses. However, the narrow margin between the generated and injected energy highlights the system's strong operational efficiency.

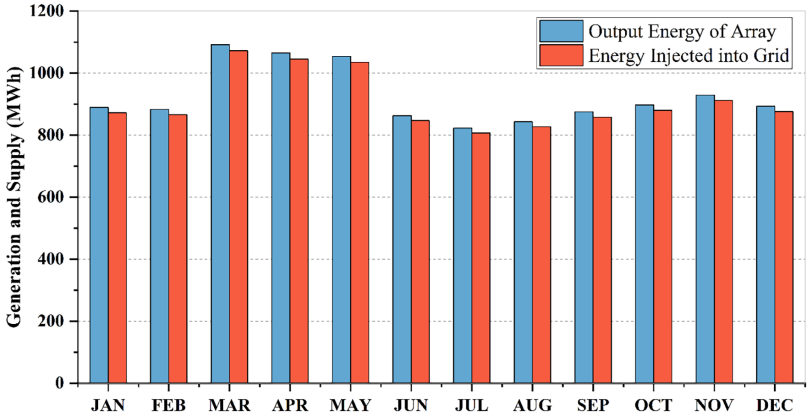

Figure 24: Monthly comparison of PV array output and energy injected into the grid.

3.2.9 Validation of Financial Metrics Using PVsyst

To enhance the accuracy of the economic analysis, key financial metrics obtained from HOMER Pro were validated using PVsyst. Table 12 shows the financial metrics of the full hybrid system from HOMER Pro and PV only from PVsyst. Although PVsyst is not intended for direct comparison with HOMER Pro due to differences in scope, it serves as a valuable tool for cross-validating the results by assessing the PV subsystem

under standard operating conditions. The consistency observed between the financial indicators from both platforms, particularly in LCOE, supports the reliability of the study's techno-economic findings.

Table 12: Economic results of homer pro for the hybrid system and PVsyst for the PV system.

Parameters	Homer Pro Simulation Results			PVsyst Simulation Results for the PV System
	Hybrid System	WT System	PV System	
LCOE	0.123	0.03	0.06	0.05
Payback year	7.4			5.4
IRR	30%			18.39%
ROI	26%			366.5%

3.3 Environmental Assessment

The environmental assessment shows that the designed hybrid system significantly reduces emissions from fossil fuel-based power generation. Table 13 presents the system's annual GHG reductions.

Table 13: Estimated annual GHG emission reduction by the hybrid system.

Gas	Quantity	Unit
Carbon Dioxide	13,729,906	kg/yr
Carbon Monoxide	0	–
Unburned Hydrocarbons	0	–
Particulate Matter	0	–
Sulfur Dioxide	59,525	kg/yr
Nitrogen Oxides	29,111	kg/yr

Table 14 presents a comparative overview of the LCOE reported in previous studies on hybrid renewable energy systems across various regions of Bangladesh. The comparison highlights the economic competitiveness of our designed hybrid system.

Table 14: Comparison of LCOE in hybrid renewable energy systems in Bangladesh.

Ref.	Study Name	LCOE (USD/kWh)
[21]	Investigation of Optimal Hybrid Energy Systems Using Available Energy Sources in a Rural Area of Bangladesh	0.239
[22]	The Best Techno-economic Aspects of the Feasibility Study Concerning the Proposed PV-Wind-hydro Hybrid System in Nilphamari, Bangladesh	0.241
[62]	Analysis of Techno-Economic-Environmental Suitability of an Isolated Microgrid System Located in a Remote Island of Bangladesh	0.340
[24]	Design of an Off-Grid Solar-Wind-Bio Hybrid Power Generation for Remote Areas of Chapainawabgonj District in Bangladesh Using Homer	0.263
[30]	Techno-economic and environmental analysis of hybrid energy systems for remote areas: A sustainable case study in Bangladesh	0.266
[25]	The Techno-Economic Feasibility Serves to Optimize the PV-Wind-Hydro Hybrid Power System at Tangail in Bangladesh	0.281

(Continued)

Table 14 (continued)

Ref.	Study Name	LCOE (USD/kWh)
[26]	Techno-economic assessment of a hybrid renewable energy storage system for rural community towards achieving sustainable development goals	0.34
[63]	Optimized design of a hybrid PV-wind-diesel energy system for sustainable development at coastal areas in Bangladesh	0.392
	Proposed PV-Wind-BESS grid-connected system	0.123

3.4 Life Cycle Assessment of the Hybrid System

An LCA evaluated the environmental impacts of the hybrid system components, including a 7.5 MW solar PV plant, 8 MWh BESS, and 6.5 MW wind. The analysis used openLCA with relevant process databases and covered material extraction, component fabrication, and transport. Fig. 25 summarizes the results. Solar PV manufacturing caused the largest share of impacts, followed by wind and BESS.

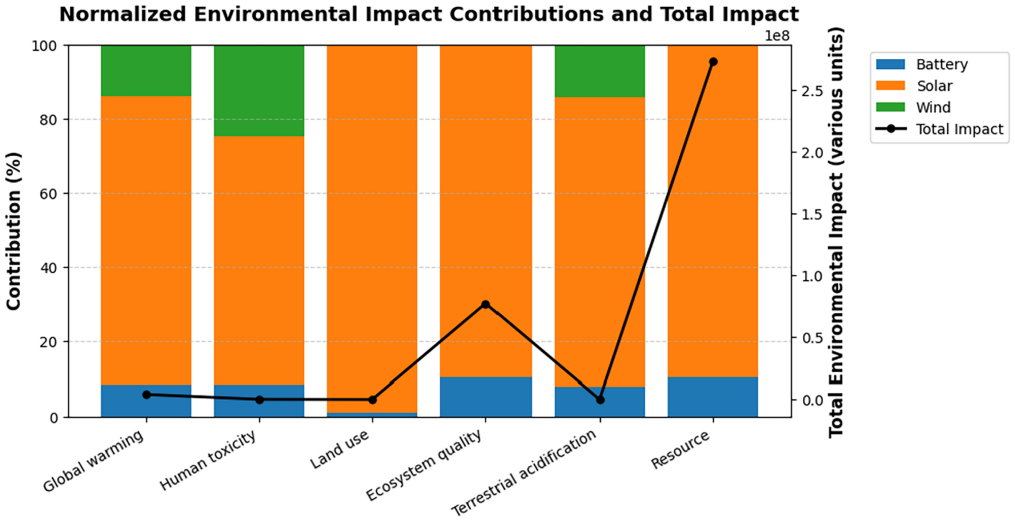

	Unit	Battery	Solar	Wind	Total
Global warming	kg CO_2 eq	3.45e+05	3.18e+06	5.63e+05	4.09e+06
Human toxicity	kg 1,4-DB eq	1.42e+04	1.14e+05	4.20e+04	1.70e+05
Land use	m^2a crop eq	2.32e+02	2.16e+04	4.68e+01	2.19e+04
Ecosystem quality	PAF·m^2·yr	8.03e+06	6.90e+07	1.22e+05	7.72e+07
Terrestrial acidification	kg SO_2 eq	6.52e+02	6.50e+03	1.17e+03	8.33e+03
Resource	MJ surplus	2.84e+07	2.44e+08	4.32e+05	2.73e+08

Figure 25: Environmental impact of producing different portions of the proposed hybrid system.

The lifetime environmental performance of the hybrid plant was compared with coal and natural gas generation producing an equivalent amount of electricity over 20 years, as shown in Table 15. The hybrid system showed lower impacts in all categories. Its total GWP (2.18×10^7 kg CO_2 eq) was about 20 times lower than coal and 11 times lower than gas generation. Human toxicity and terrestrial acidification were reduced by over 90%, while ecosystem quality impact declined by approximately 80%–90%.

Although land use for renewable installations was marginally higher, the overall life cycle impacts per unit of electricity were substantially lower than those of fossil-based generation. These results confirm

that, despite higher emissions during manufacturing, the hybrid system achieves significant environmental advantages throughout its operational lifetime.

Table 15: Environmental impact comparison of the proposed hybrid system and the conventional system.

Indicator	Unit	Proposed	Coal		Gas	
			per Year	Life Time	per Year	Life Time
Global warming	kg CO_2 eq	4.089×10^6	2.181×10^7	4.362×10^8	1.179×10^7	2.358×10^8
Human toxicity	kg 1,4-DB eq	1.697×10^5	8.732×10^5	1.746×10^7	4.719×10^5	9.438×10^6
Land use	m^2a crop eq	2.186×10^4	1.909×10^4	3.818×10^5	1.032×10^4	2.064×10^5
Ecosystem quality	PAF $*$ m^2 yr	7.719×10^7	2.313×10^7	4.626×10^8	1.25×10^7	2.5×10^8
Terrestrial acidification	kg SO_2 eq	8325.9	3.43×10^4	6.86×10^5	1.854×10^4	3.708×10^5
Resource	MJ surplus	2.731×10^8	8.187×10^7	1.637×10^9	4.425×10^7	8.85×10^8

4 Limitation and Future Scope

- While the analysis of the existing Sirajganj Solar PV Power Plant was conducted using practical operational data, the proposed hybridization relies heavily on software-based simulations. Although these platforms offer reliable modeling, they cannot fully address all practical constraints and dynamic operational challenges. Hardware-level testing and field implementation are necessary to validate the integration of solar PV and BESS into the PV system under real-world operating conditions.
- In this study, land cost was not considered in the economic analysis, as the existing solar PV system was established on publicly owned land made available at no cost. However, in future hybrid renewable energy projects, particularly in areas where land must be purchased or leased, land acquisition costs may significantly affect key economic indicators such as NPC, LCOE, and payback period. Therefore, future analyses should incorporate land pricing to reflect more realistic economic feasibility.
- Socio-economic impacts, including employment generation, stakeholder engagement, and public perception, were also beyond the scope of this study. These aspects are critical to the large-scale adoption of hybrid renewable energy systems. Future work should integrate social and policy considerations to provide a broader perspective on feasibility and sustainability.

5 Conclusion

This study presents the techno-economic feasibility of converting an existing grid-connected solar PV plant into a hybrid renewable energy system by integrating wind energy and BESS. MATLAB Simulink and DIgSILENT PowerFactory were used to optimize key technical challenges such as intermittency, grid stability, and power quality. Technical optimizations including harmonic distortion filtering, fault detection and isolation, and frequency regulation, played a crucial role in improving system performance. Quantitatively, the proposed hybrid system reduced the RoCoF by 22% and THD from 106.5% to 2.14% compared to the standalone PV plant. It demonstrates compliance with ENTSO-E grid codes. HOMER Pro compared six configurations and determined the optimal setup. The selected configuration, which includes 7.5 MW of solar PV, 6.5 MW of wind, and an 8 MWh lithium-ion BESS, achieves an NPC of $34.5 million and a competitive LCOE of $0.123/kWh. A Monte Carlo-based sensitivity analysis confirms the robustness of the results. PVsyst revealed a strong performance ratio of 76.6% and provided a detailed energy-loss distribution. The study also performs an LCA, which shows the project significantly reduces greenhouse gas emissions, with a global warming potential approximately 20 times lower than coal and 11 times lower than natural gas,

contributing to long-term environmental sustainability. The findings can serve as a valuable reference for planning future hybrid renewable energy projects.

Acknowledgement: The authors would like to acknowledge the support provided by the Deanship of Scientific Research, King Faisal University, Al-Ahsa, Saudi Arabia.

Funding Statement: This work was supported by the Deanship of Scientific Research, Vice Presidency for Graduate Studies and Scientific Research, King Faisal University, Saudi Arabia [Grant No. KFU262120].

Author Contributions: Conceptualization, Riad Mollik Babu and Md Shafiul Alam; methodology, Riad Mollik Babu and Md Shafiul Alam; software, Riad Mollik Babu and Md. Hasibur Rahman; validation, Md Shafiul Alam, Mohammad Ali and Md. Alamgir Hossain; formal analysis, Md. Arifuzzaman; investigation, Riad Mollik Babu and Md Shafiul Alam; resources, Mohammad Ali; data curation, Md. Alamgir Hossain; writing—original draft preparation, Md. Arifuzzaman; writing—review and editing, Md Shafiul Alam; visualization, Md. Hasibur Rahman; supervision, Md Shafiul Alam; project administration, Riad Mollik Babu; funding acquisition, Md Shafiul Alam, Mohammad Ali, Md. Alamgir Hossain and Md. Arifuzzaman. All authors reviewed and approved the final version of the manuscript.

Availability of Data and Materials: Data will be made available upon reasonable request from the corresponding author.

Ethics Approval: Not applicable.

Conflicts of Interest: The authors declare no conflicts of interest.

References

1. IRENA. Renewable capacity statistics 2025. Abu Dhabi, United Arab Emirates: International Renewable Energy Agency; 2025.
2. Mollik Babu R, Alam MS, Islam A, Kamrul Islam M. Toward sustainable and clean energy futures: a techno-economic review of solar PV systems, challenges, and opportunities. IEEE Access. 2025;13(20):169720–57. doi:10.1109/ACCESS.2025.3614771.
3. Mohammadi F, Neagoe M. Emerging issues and challenges with the integration of solar power plants into power systems. In: Solar energy conversion in communities. Berlin/Heidelberg, Germany: Springer; 2020. p. 157–73. doi:10.1007/978-3-030-55757-7_11.
4. Gayen D, Chatterjee R, Roy S. A review on environmental impacts of renewable energy for sustainable development. Int J Environ Sci Technol. 2024;21(5):5285–310. doi:10.1007/s13762-023-05380-z.
5. Gao Y, Meng Y, Dong G, Ma S, Miao C, Xiao J, et al. The wind-solar hybrid energy could serve as a stable power source at multiple time scale in China mainland. Energy. 2024;305:132294. doi:10.1016/j.energy.2024.132294.
6. Babu RM, Islam MS, Basher E, Rahman MH. Enhancing solar PV system performance in Bangladesh: a comprehensive analysis of the Sarishabari solar plant and strategic recommendations. Int J Energy Prod Manag. 2025;10(1):1–11. doi:10.18280/ijepm.100101.
7. Amrollahi MH, Bathaee SMT. Techno-economic optimization of hybrid photovoltaic/wind generation together with energy storage system in a stand-alone micro-grid subjected to demand response. Appl Energy. 2017;202(7):66–77. doi:10.1016/j.apenergy.2017.05.116.
8. Shezan SKA, Das N, Mahmudul H. Techno-economic analysis of a smart-grid hybrid renewable energy system for Brisbane of Australia. Energy Proc. 2017;110:340–5. doi:10.1016/j.egypro.2017.03.150.
9. Li Y, Xu Z, Xiong L, Song G, Zhang J, Qi D, et al. A cascading power sharing control for microgrid embedded with wind and solar generation. Renew Energy. 2019;132(1):846–60. doi:10.1016/j.renene.2018.07.150.
10. Lamedica R, Santini E, Ruvio A, Palagi L, Rossetta I. A MILP methodology to optimize sizing of PV-Wind renewable energy systems. Energy. 2018;165(5):385–98. doi:10.1016/j.energy.2018.09.087.

11. Gulzar MM, Iqbal A, Sibtain D, Khalid M. An innovative converterless solar PV control strategy for a grid connected hybrid PV/wind/fuel-cell system coupled with battery energy storage. IEEE Access. 2023;11(4):23245–59. doi:10.1109/ACCESS.2023.3252891.
12. Babu RM. Forecasting and techno-economic optimization of residential PV-battery systems: a synergistic approach for system enhancement. Next Mater. 2026;11(1):101968. doi:10.1016/j.nxmate.2026.101968.
13. Babu RM, Paul D, Islam MS, Hossain MM. Techno-economic analysis of integrating wind and BESS into an existing grid-tied solar PV system. In: Proceedings of the 2025 IEEE International Conference on Environment and Electrical Engineering and 2025 IEEE Industrial and Commercial Power Systems Europe (EEEIC/I&CPS Europe); 2025 Jul 15–18; Chania, Crete, Greece. doi:10.1109/EEEIC/ICPSEurope64998.2025.11169141.
14. Yang H, Wei Z, Lou C. Optimal design and techno-economic analysis of a hybrid solar-wind power generation system. Appl Energy. 2009;86(2):163–9. doi:10.1016/j.apenergy.2008.03.008.
15. Jha N, Prashar D, Rashid M, Khanam Z, Nagpal A, AlGhamdi AS, et al. Energy-efficient hybrid power system model based on solar and wind energy for integrated grids. Math Probl Eng. 2022;2022:4877422. doi:10.1155/2022/4877422.
16. Islam MA, Naushad Ali MM, Al Mamun A, Shahadat Hossain M, Maruf MH, Shihavuddin ASM. Optimizing energy solutions: a techno-economic analysis of solar-wind hybrid power generation in the coastal regions of Bangladesh. Energy Convers Manag X. 2024;22(2):100605. doi:10.1016/j.ecmx.2024.100605.
17. Prasad AR, Natarajan E. Optimization of integrated photovoltaic-wind power generation systems with battery storage. Energy. 2006;31(12):1943–54. doi:10.1016/j.energy.2005.10.032.
18. Khan FA, Pal N, Saeed SH, Yadav A. Techno-economic and feasibility assessment of standalone solar Photovoltaic/Wind hybrid energy system for various storage techniques and different rural locations in India. Energy Convers Manag. 2022;270(8):116217. doi:10.1016/j.enconman.2022.116217.
19. Braff WA, Mueller JM, Trancik JE. Value of storage technologies for wind and solar energy. Nature Clim Change. 2016;6(10):964–9. doi:10.1038/nclimate3045.
20. Babu RM, Basher E. Performance evaluation and economic analysis of a grid-connected solar power plant: a case study of engreen sarishabari solar plant ltd. Bangladesh Ecol Eng Environ Technol. 2024;25(5):220–34. doi:10.12912/27197050/185934.
21. Rashid F, Hoque ME, Aziz M, Sakib TN, Islam MT, Robin RM. Investigation of optimal hybrid energy systems using available energy sources in a rural area of Bangladesh. Energies. 2021;14(18):5794. doi:10.3390/en14185794.
22. Islam MS, Noman NA, Habib MA. The best techno-economic aspects of the feasibility study concerning the proposed PVWind-hydro hybrid system in Nilphamari. Bangladesh Int J Educ Manag Eng. 2022;12(5):24–37. doi:10.5815/ijeme.2022.05.04.
23. Nandi SK, Ghosh HR. A wind-PV-battery hybrid power system at Sitakunda in Bangladesh. Energy Policy. 2009;37(9):3659–64. doi:10.1016/j.enpol.2009.04.039.
24. Saifullah MK, Halder R, Afroz S, Shatil AH, Ahmed KF. Design of an off-grid solar-wind-bio hybrid power generation for remote areas of chapainawabgonj district in Bangladesh using Homer. In: Proceedings of the 2023 3rd International Conference on Robotics, Electrical and Signal Processing Techniques (ICREST); 2023 Jan 7–8; Dhaka, Bangladesh. doi:10.1109/ICREST57604.2023.10070032.
25. Ahamed Noman N, Sariful Islam M, Ahsan Habib M, Kumar Debnath S. The techno-economic feasibility serves to optimize the pv-wind-hydro hybrid power system at Tangail in Bangladesh. Educ Manag Eng. 2023;13(3):19–32. doi:10.5815/ijeme.2023.03.03.
26. Wali SB, Hannan MA, Ker PJ, Abd Rahman MS, Tiong SK, Begum RA, et al. Techno-economic assessment of a hybrid renewable energy storage system for rural community towards achieving sustainable development goals. Energy Strategy Rev. 2023;50(1):101217. doi:10.1016/j.esr.2023.101217.
27. Al Mamun A, Hossain Lipu MS, Islam ZU, Barua S, Rahman T, Karim TF, et al. Sustainable renewable energy integration on expressways in Bangladesh: a techno-economic, environmental, and sensitivity analysis of a grid-connected hybrid system. Energy Convers Manag X. 2025;26:101020. doi:10.1016/j.ecmx.2025.101020.

28. Ali MF, Biswas D, Sheikh MRI, Al Mamun A, Hossen MJ. Techno-economic optimization of battery storage technologies for off-grid hybrid microgrids in multiple rural locations of Bangladesh. Front Energy Res. 2025;13:1654615. doi:10.3389/fenrg.2025.1654615.
29. Chowdhury P, Islam T, Agyekum EB. Techno-economic and multicriteria analysis of grid-connected energy systems for hydrogen production: a case study from Bangladesh. Int J Hydrogen Energy. 2025;109:95–114. doi:10.1016/j.ijhydene.2025.02.034.
30. Mojumder MFH, Islam T, Chowdhury P, Hasan M, Takia NA, Chowdhury NUR, et al. Techno-economic and environmental analysis of hybrid energy systems for remote areas: a sustainable case study in Bangladesh. Energy Convers Manag X. 2024;23:100664. doi:10.1016/j.ecmx.2024.100664.
31. Ishraque MF, Shezan SA, Ali MM, Rashid MM. Optimization of load dispatch strategies for an islanded microgrid connected with renewable energy sources. Appl Energy. 2021;292(4):116879. doi:10.1016/j.apenergy.2021.116879.
32. Biswas D, Ali MF, Saha M, Alam MS, Ali M, AlAqil MA, et al. Techno-economic optimization, sensitivity analysis and stability evaluation of a high-renewable hybrid microgrid for rural Bangladesh. Sci Rep. 2026;16(1):7695. doi:10.1038/s41598-026-38328-7.
33. Rasel Ahmed M, Nimul Hasan M, Shezan SA, Fatin Ishraque M, Das BK, Tushar MSHK. Assessment of a grid-connected microgrid for suburban areas and EV loads with battery storage during planned grid outages using DIgSILENT powerfactory. Electr Eng. 2025;107(12):15069–98. doi:10.1007/s00202-025-03313-2.
34. Ali MF, Azam ME, Shezan SA, Alam MS, Hossain MA, Ali M, et al. Techno-economic feasibility study of hydrogen storage in enhancing the reliability of a renewable-based microgrid for residential applications. Sci Rep. 2025;15(1):43473. doi:10.1038/s41598-025-28383-x.
35. Khan MJ, Iqbal MT, Mahboob S. A wind map of Bangladesh. Renew Energy. 2004;29(5):643–60. doi:10.1016/j.renene.2003.10.002.
36. Sustainable and renewable energy development authority (SREDA)-power division; ministry of power, energy & mineral resources [Internet]. [cited 2025 Nov 3]. Available from: https://sreda.gov.bd/.
37. Bangladesh power development board [Internet]. [cited 2025 Nov 3]. Available from: https://bpdb.gov.bd/.
38. Bangladesh inflation rate [Internet]. [cited 2025 Apr 20]. Available from: https://tradingeconomics.com/bangladesh/inflation-cpi.
39. Karim Miah MA, Rakib N, Habib MA, Hasanuzzaman M, Saha S. Techno-economic analysis and environmental impact assessment of 3 MW photovoltaic power plant in Bangladesh: a case study based on real data. Environ Dev Sustain. 2023;25(12):15205–23. doi:10.1007/s10668-022-02634-7.
40. POWERing the future of energy, infrastructure, and agroclimatology, NASA POWER|Homepage [Internet]. [cited 2025 Nov 3]. Available from: https://power.larc.nasa.gov/.
41. Meteonorm Version 8-Meteonorm (en) [Internet]. [cited 2025 Nov 3]. Available from: https://mn8.meteonorm.com/en/meteonorm-version-8.
42. Bangladesh meteorological department [Internet]. [cited 2025 Nov 3]. Available from: https://live6.bmd.gov.bd/.
43. LG solar module premium products|LG USA business [Internet]. [cited 2025 Jul 4]. Available from: https://www.lg.com/us/business/solar-panels/view-all.
44. 100 kW wind turbine-horizontal axis [Internet]. [cited 2025 Jul 4]. Available from: https://www.pvmars.com/product/100kw-wind-turbine/.
45. The best 100 kW wind turbines–PMDD technology|NPS [Internet]. [cited 2026 Apr 18]. Available from: https://northernpower.com/100kw-wind-turbines/.
46. Liu Y, Yao L, Zhao DW, Qian M, Jiang D. Steady-state modelling of VSC MTDC for power system analysis in DIgSILENT power factory. In: Proceedings of the 2018 China International Conference on Electricity Distribution (CICED); 2018 Sep 17–19; Tianjin, China. doi:10.1109/CICED.2018.8592494.
47. Eidiani M. Modeling renewable energy resources using DIgSILENT PowerFactory software. In: Power systems operation with 100% renewable energy sources. Amsterdam, The Netherlands: Elsevier; 2024. p. 165–202. doi:10.1016/b978-0-443-15578-9.00013-3.
48. Mosobi RW, Chichi T, Gao S. Power quality analysis of hybrid renewable energy system. Cogent Eng. 2015;2(1):1005000. doi:10.1080/23311916.2015.1005000.

49. Khalil L, Liaquat Bhatti K, Arslan Iqbal Awan M, Riaz M, Khalil K, Alwaz N. Optimization and designing of hybrid power system using HOMER pro. Mater Today Proc. 2021;47:S110–5. doi:10.1016/j.matpr.2020.06.054.
50. Saleh AH, Aftan AO. The analysis and techno-economic of hybrid renewable energy system using HOMER PRO simulation. AIP Conf Proc. 2025;3350(1):080002. doi:10.1063/5.0299805.
51. Baqir M, Channi HK. Analysis and design of solar PV system using Pvsyst software. Mater Today Proc. 2022;48:1332–8. doi:10.1016/j.matpr.2021.09.029.
52. El Kassar R, El Rassy E, Py X, Al Takash A, Hammoud M, El Saleh A. Cradle-to-grave life cycle assessment of a commercial rooftop PV system with complete BOS in west Africa: recipe-based LCA using OpenLCA. In: Proceedings of the 2025 Sixth International Conference on Advances in Computational Tools for Engineering Applications (ACTEA); 2025 Sep 24–26; Zouk Mosbeh, Lebanon. doi:10.1109/ACTEA66485.2025.11189967.
53. openLCA [Internet]. [cited 2026 Apr 18]. Available from: https://www.openlca.org/.
54. van Zelm R, Hennequin T, Huijbregts MAJ. Performing life cycle impact assessment with the midpoint and endpoint method ReCiPe. Nat Protoc. 2025;20(12):3400–11. doi:10.1038/s41596-025-01207-y.
55. Huijbregts MAJ, Steinmann ZJN, Elshout PMF, Stam G, Verones F, Vieira M, et al. ReCiPe2016: a harmonised life cycle impact assessment method at midpoint and endpoint level. Int J Life Cycle Assess. 2017;22(2):138–47. doi:10.1007/s11367-016-1246-y.
56. Rybaczewska-Błażejowska M, Jezierski D. Comparison of ReCiPe 2016, ILCD 2011, CML-IA baseline and IMPACT 2002+ LCIA methods: a case study based on the electricity consumption mix in Europe. Int J Life Cycle Assess. 2016;29(10):1799–817. doi:10.1007/s11367-024-02326-6.
57. CML-IA characterisation factors-leiden university [Internet]. [cited 2026 Apr 18]. Available from: https://www.universiteitleiden.nl/en/research/research-output/science/cml-ia-characterisation-factors.
58. Li J, Hua Z, Tian L, Chen P, Dong H. Optimal capacity allocation for life cycle multiobjective integrated energy systems considering capacity tariffs and eco-indicator 99. Sustainability. 2024;16(20):8930. doi:10.3390/su16208930.
59. openLCA Nexus: the source for LCA data sets [Internet]. [cited 2026 Apr 18]. Available from: https://nexus.openlca.org/database/ELCD.
60. UCTE. P1-policy 1: load-frequency control and performance. Brussels, Belgium: Union for the Co-ordination of Transmission of Electricity; 2009.
61. [Press Release] ENTSO-E technical report on the January 2019 significant frequency deviations in Continental Europe [Internet]. [cited 2026 Apr 18]. Available from: https://www.entsoe.eu/news/2019/05/28/entso-e-technical-report-on-the-january-2019-significant-frequency-deviations-in-continental-europe/.
62. Masrur H, Howlader HOR, Elsayed Lotfy M, Khan KR, Guerrero JM, Senjyu T. Analysis of techno-economic-environmental suitability of an isolated microgrid system located in a remote island of Bangladesh. Sustainability. 2020;12(7):2880. doi:10.3390/su12072880.
63. Rashid S, Rana S, Shezan SKA, Karim SAB, Anower S. Optimized design of a hybrid PV-wind-diesel energy system for sustainable development at coastal areas in Bangladesh. Environ Prog Sustain Energy. 2017;36(1):297–304. doi:10.1002/ep.12496.